



**HAL**  
open science

## Pastoralism increased vulnerability of a subalpine catchment to flood hazard through changing soil properties

Manon Bajard, Jérôme Poulenard, Pierre Sabatier, Yann Bertrand, Christian Crouzet, Gentile Francesco Ficetola, Claire Blanchet, Erwan Messenger, Charline Giguet-Covex, Ludovic Gielly, et al.

### ► To cite this version:

Manon Bajard, Jérôme Poulenard, Pierre Sabatier, Yann Bertrand, Christian Crouzet, et al.. Pastoralism increased vulnerability of a subalpine catchment to flood hazard through changing soil properties. *Palaeogeography, Palaeoclimatology, Palaeoecology*, 2020, 10.17632/j9x7yhev4.1 . hal-02395553

**HAL Id: hal-02395553**

**<https://hal.science/hal-02395553>**

Submitted on 7 Mar 2022

**HAL** is a multi-disciplinary open access archive for the deposit and dissemination of scientific research documents, whether they are published or not. The documents may come from teaching and research institutions in France or abroad, or from public or private research centers.

L'archive ouverte pluridisciplinaire **HAL**, est destinée au dépôt et à la diffusion de documents scientifiques de niveau recherche, publiés ou non, émanant des établissements d'enseignement et de recherche français ou étrangers, des laboratoires publics ou privés.



Distributed under a Creative Commons Attribution - NonCommercial 4.0 International License

1 **Pastoralism increased vulnerability of a subalpine catchment to flood hazard**  
2 **through changing soil properties**

3 Manon Bajard<sup>1,2</sup>, Jérôme Poulénard<sup>2</sup>, Pierre Sabatier<sup>2</sup>, Yann Bertrand<sup>2</sup>, Christian Crouzet<sup>3</sup>, Gentile  
4 Francesco Ficetola<sup>4,5</sup>, Claire Blanchet<sup>2</sup>, Erwan Messenger<sup>2</sup>, Charline Giguët-Covex<sup>2</sup>, Ludovic Gielly<sup>4</sup>,  
5 Delphine Rioux<sup>4</sup>, Wentao Chen<sup>4</sup>, Emmanuel Malet<sup>2</sup>, Anne-Lise Develle<sup>2</sup>, and Fabien Arnaud<sup>2</sup>

6

7 <sup>1</sup>Centre for Earth Evolution and Dynamics, University of Oslo, PO Box 1028, Blindern, 0315 Oslo,  
8 Norway

9 <sup>2</sup>Univ. Grenoble Alpes, Univ. Savoie Mont Blanc, CNRS, EDYTEM, 73000 Chambéry, France

10 <sup>3</sup>ISTerre, Univ. Grenoble Alpes, Univ. Savoie Mont Blanc, CNRS, 73000 Chambéry, France

11 <sup>4</sup>LECA, CNRS UMR 5553, Université Grenoble Alpes, 38041 Grenoble, France

12 <sup>5</sup>Department of Environmental Science and Policy, Università degli Studi di Milano, Milan 20133, Italy

13

14 Corresponding authors : Manon Bajard: [manon@geo.uio.no](mailto:manon@geo.uio.no)

15 **Abstract**

16 Soil erosion is strongly linked to both precipitation patterns and land-use. We examine the  
17 effects of erosion and its drivers (*i.e.* human or/and climate) on soil evolution from the study of  
18 lacustrine archives in the northern French Alps. Multi-proxy analyses of the Lake Gers sediment  
19 sequence combined with the study of soils and rocks of its catchment allowed to reconstruct its  
20 evolution over the past 4.6 kyr. This included <sup>14</sup>C dating, short-lived radionuclides, geochemistry, loss  
21 on ignition, grain-size analyses, as well as plant and mammal DNA analyses. A total of 127  
22 instantaneous deposits were identified among the continuous sedimentation in the lake and 93 were

23 interpreted as flood deposits. Erosion was quantified for the whole catchment considering both the  
24 continuous sedimentation and the flood deposit thicknesses.

25 The catchment is mainly formed by andesitic sandstones over which Andosols and Podzols  
26 can develop. However, low weathered materials from colluviation constitute the main input to the  
27 lake.

28 Four main phases of changes in soil weathering were recorded by increases in  $K_2O/TiO_2$   
29 ratios, associated with an increase in both erosion and flood-frequency. Two phases were associated  
30 with climate cooling in the Western Alps, from 2.65 to 2.5 and from 1.45 to 1.3 cal kyr BP. The two  
31 others (1.9-1.75 and 0.9-0.4 cal kyr BP) were triggered with deforestation, with cow grazing during  
32 the Roman period, and with grazing of cows, sheep and goats during the Medieval period, amplified  
33 by the onset of the Little Ice Age. The increase in erosion and flood frequency after 950 cal yr BP  
34 indicates substantial damages to soils of the catchment including increase of their erodibility over the  
35 last millennia.

36

37 Key-words: lake sediments, pedogenesis, weathering, pastoralism, climate, erodibility.

38

## 39 1. Introduction

40

41 Erosion is a natural process, commonly occurring in mountain areas due to steep slopes and high  
42 precipitation (Verheijen et al., 2009). Torrential flooding transport mechanisms are often studied for  
43 flood hazards and for climatic impacts, which are exacerbated by snow melting in spring or intense  
44 stormy rainfall in summer and fall (Noren et al., 2002; Wilhelm et al., 2012; Sabatier et al., 2017;  
45 Wilhelm et al., 2018). Few studies focus on the long term effects of flood-triggered erosion on soil  
46 evolution despite the fact that landscape, that are based on the soil cover, may be threatened by

47 flood events. Soils provide numerous ecosystem services, including supporting, provisioning and  
48 regulating services, as food production, regulation of climate disruption by carbon storage and flood  
49 mitigation (Daily et al., 1997; MEA, 2005; Adhikari and Hartemink, 2016). The loss of soil thickness is  
50 frequently associated to loss of soil properties like structure or organic matter content (Stacy et al.,  
51 2015; Wang et al., 2017). This can decrease the potential of water infiltration and storage and favor  
52 surface runoff, through Horton overland flow, thus further increasing erosion (Bailey et al., 1934).  
53 The loss of soils in upstream mountain catchments induces more direct and rapid concentration of  
54 waters and thus can have strong effect on valley flooding, where infrastructures and housing are  
55 concentrated. This displacement of soil and sediments can also result in deep hydrological changes in  
56 the catchment. The consequences of floods are thus doubled, with the potential mobilization of large  
57 amount of soil associated with ecological and economical losses, as well as the transfer of large  
58 amount of water downstream, threatening societies. If flooding are necessary triggered by  
59 precipitation, their effects on erosion can be increased according to the conditions of the catchment,  
60 especially in response to human-induced modifications (Cosandey et al., 2005; Giguët-Covex et al.,  
61 2011; Brisset et al., 2017). Therefore, it is necessary to dissociate what is climate or human induced  
62 in flood related erosion, and take interest in land use modifications.

63 Both the number and intensity of extreme precipitations and thus, flood events, are expected to  
64 increase with the climate warming in several places in the world and especially in mountainous areas  
65 (Giorgi et al., 2016). Consequences of the global warming will also affect lands and agriculture  
66 systems as highlighted recently by the IPCC Special Report on Climate Change and Land (IPCC, 2019).  
67 In this context, it becomes essential to understand how soils can react and be disrupted by flood and  
68 land use change to adapt environmental practices and management in the upstream, thereby  
69 ensuring safe living accommodation and sustainability of the agro-pastoral practices. Upstream areas  
70 are usually neglected in risk prevention plans or adaptation to climate change because they are  
71 considered as natural areas and located usually far from human properties values.

72 Paleo-environmental reconstructions from lake sediments offer the opportunities to study at the  
73 same time soil evolution, flood-frequency and effect of human activities on long time-scale (Giguet-  
74 Covex et al., 2011, 2014; Arnaud et al., 2016; Brisset et al., 2017). Lake sediment archives are useful  
75 to reconstruct past flood events, especially in mountainous areas (Noren et al., 2002; Moreno et al.,  
76 2008; Wilhelm et al., 2012; Wirth et al., 2013; Sabatier et al., 2017; Fouinat et al., 2017a; Wilhelm et  
77 al., 2019). They also can be used to reconstruct past land use and agricultural activities from pollen  
78 and non-pollen palynomorph analyses (Doyen and Etienne, 2017) and from plant and mammal DNA  
79 (*e.g.*, animal husbandry) (Giguet-Covex et al., 2014; Parducci et al., 2017; Sabatier et al., 2017; Bajard  
80 et al., 2017b). Soil evolution is reconstructed from the comparison between the lake archives and the  
81 current soils (Ewing and Nater, 2002; Mourier et al., 2008; Giguet-Covex et al., 2011; Bajard et al.,  
82 2017b).

83 Here we present a study based on a lake sediment sequence of the Northern French Alps with  
84 the objectives to i) identify flood deposits and establish a flood chronicle, ii) understand the soil  
85 evolution, applying a source-to-sink approach (*i.e.*, combining catchment samples and lake sediment  
86 analyses) and to iii) link soil evolution and flood-frequency with external anthropic and/or climate  
87 forcing.

88

## 89 2. Materials and methods

### 90 2.1 Study site

91 Lake Gers (46°1'36"N, 6°43'45"E, 1540 m a.s.l.) is located in the Northern French Alps (Fig.  
92 1a) on the municipality of Samoëns in the Giffre river Valley. The area of the lake is 0.05 km<sup>2</sup> and its  
93 maximum depth is 5.6 m (Sesiano, 1993). The lake level decreases of 2 m between spring and  
94 summer because of loss of water under the lake (Fig. 1b). The lake is fed by a temporary stream that  
95 mainly drains the west side of the catchment. The catchment covers an area of 5 km<sup>2</sup> and rises up to  
96 2385 m a.s.l. (Fig. 1c). The lake is of glacial origin and is part of the Giffre river catchment.

97           According to the weather observation network of the alpine massif (ROMMA), the mean  
98   temperatures at Arâches-La Frasse, located at 8 km west from Lake Gers at 1120 m and corrected of  
99   an altitudinal gradient of  $-0.5^{\circ}\text{C}/100\text{ m}$  for Lake Gers altitude, range from  $-1.2^{\circ}\text{C}$  in winter to  $13.0^{\circ}\text{C}$  in  
100   summer (these values represent averages for 2011-2017). Precipitations are approximately 1500 mm  
101   per year. Snow covers the area from December to April, and the lake is ice-covered during winter.  
102   Avalanches fall out every winter and early spring, especially from the west side of the lake, and can  
103   reach the lake.

104           The bedrock of the catchment is dominated by Taveyannaz sandstones of Eocene-Oligocene  
105   ages (Fig. 1c), which are composed by approximately 80 % of volcanic materials associated with a  
106   carbonated matrix (Martini, 1966). Within the sandstones, carbonated marly levels can outcrop in  
107   some points of the catchment (*e.g.*, GERS3, GERS4).

108           *Picea abies* is the main tree species covering the east side of the lake (Fig. 1c and 1d).  
109   Pastured grasslands cover the south edge of the lake and the upstream of the catchment with  
110   punctual areas colonized by *Ericaceae* (*Vaccinium myrtillus*, *Vaccinium uliginosum*, *Rhododendron*  
111   *ferrugineum*). Alder (*Alnus viridis*) concentrates in the middle of the catchment and in avalanche  
112   areas (Figs 1c and 1d).

113   **[insert FIGURE 1]**

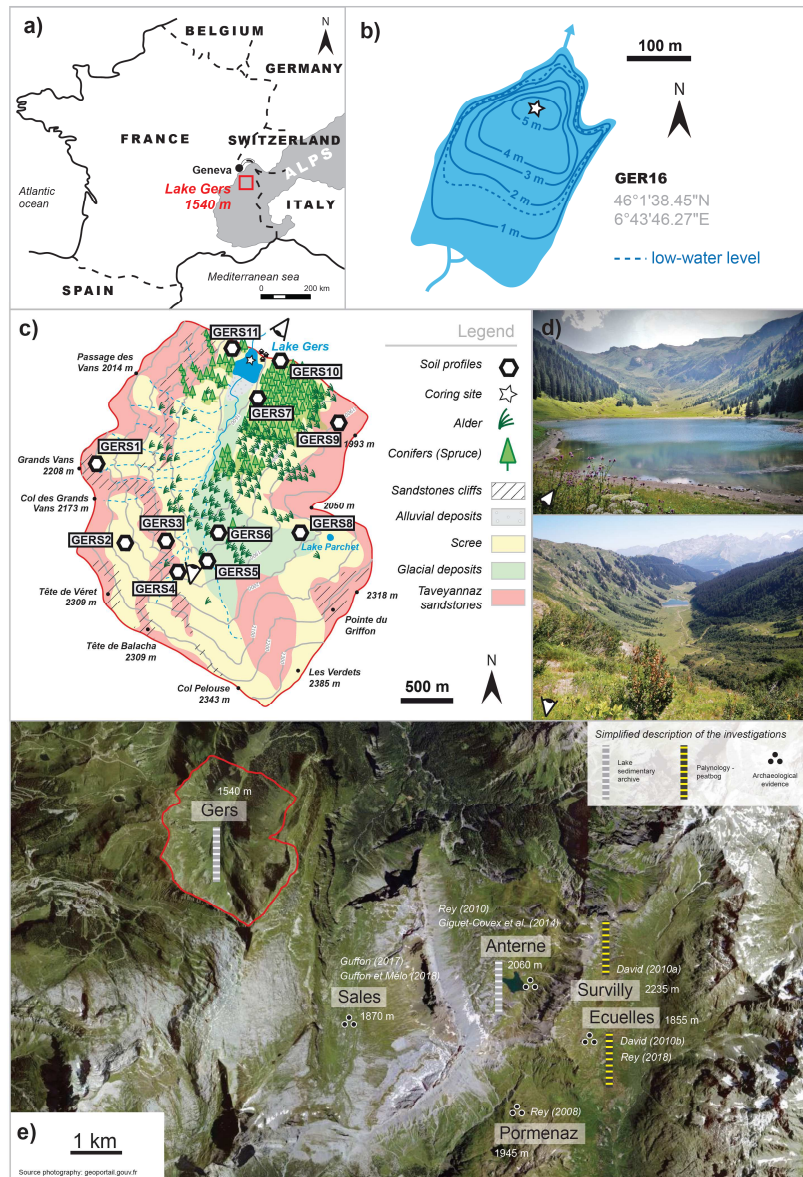


**Figure 1.** Location of Lake Gers in the Western Alps (a) with the bathymetry of the lake (b) adapted from Sesiano (1993), the simplified geological map of the catchment with the location of the soil profiles (c), the views from the north and south sides of the lake catchment (d) and locations of the nearest sites referenced in the discussion (e).

114

## 115 2.2 Soil sampling

116 Eleven soil profiles (GERS1 to 11) were realized in Lake Gers catchment to characterize the  
 117 major soil types. Soil profiles were described with color, texture, structure and HCl effervescence  
 118 test. The FAO (Food and Agriculture Organization) soil classification (WRB - FAO, 2014) and the  
 119 Guidelines for soil description (FAO, 2006) were used for horizon and soil denominations. At least  
 120 one sample was collected per horizons and sieved to 2 mm for further laboratory analyses. When it  
 121 was possible, samples for density estimation were taken with a cylinder. Parent materials from these

122 soils were also collected for geochemical comparison. Soil pH (n=3) were measured for each horizon  
123 with a 1:5 soil-water ratio.

### 124 *2.3 Lake sediment cores*

125 Two coring campaigns were undertaken to retrieve sediments from the deepest part of Lake  
126 Gers in winter 2015 and winter 2016. Short gravity cores were taken in 2015 from the ice-covered  
127 surface to provide a well-preserved water-sediment interface. Two longer overlapping sections  
128 (GER16-I and GER16-II) that are approximately 6 m each in length were retrieved in 2016 (Fig. 1b)  
129 using an Uwitec piston coring device. The cores were split into two halves. Each half was described in  
130 detail, and pictures were taken with a 20-pixel.mm<sup>-1</sup> resolution. The lithological description of the  
131 cores allowed the identification of different sedimentary units. A composite profile of 5.8 m (GER16)  
132 was built with lithological correlation from a short gravity core (GER15\_P3) obtained in 2015 (IGSN  
133 code: IEFRA05HV; *IGSN codes refer to an open international database, www.geosamples.org*) and the  
134 two sedimentary sections obtained during the 2016 coring. One half of the core was used for non-  
135 destructive analysis (*i.e.*, XRF core scanner) and the other half for sampling and performed  
136 destructive analysis.

### 137 *2.4 Analysis performed on both catchment and lake sediment samples*

#### 138 *2.4.1 Loss on ignition*

139 Loss on ignition (LOI) analysis was performed on both the soil samples and sediments, every  
140 2 cm all along the sediment sequence to estimate the organic matter (OM) and carbonate contents  
141 following the procedure described in Heiri et al. (2001). A measure of density was also realized every  
142 2 cm on the sediment core, by sampling and weighting known volume of sediment before the LOI  
143 measures.

#### 144 *2.4.2 P-XRF mineral geochemistry*

145 A portable ED-XRF spectrometer (S1 TITAN Bruker) was used on soils, rocks and lake  
146 sediments to have a quantitative and comparative measurement of major elements, which were

147 expressed as relative percentages of oxides. Analysis of gently crushed soil and sediment and crushed  
148 rocks samples was performed through a 4- $\mu\text{m}$ -thick Ultralene film in a 32-mm-diameter plastic cup.  
149 The samples were triplicated and analyzed over 60 s using the GeoChem Standard instrument's  
150 internal calibration mode (Shand and Wendler, 2014). The standard deviations of the replicates were  
151 lower than the instrument errors, which were thus conserved as measurement uncertainties. The  
152 total contents of Si, Fe Al and Mn were estimated from  $\text{SiO}_2$ ,  $\text{Fe}_2\text{O}_3$ ,  $\text{Al}_2\text{O}_3$  and MnO contents,  
153 respectively. Principal component analysis (PCA) was performed on the P-XRF geochemical data from  
154 rock and soil samples in order to identify similar rock samples and associated similar soil processes.  
155 Analyses were performed using R 2.13.1 (R Development Core Team, 2011).

## 156 *2.5 Analysis performed only on lake sediments*

### 157 *2.5.1 XRF Core Scanner*

158 The relative contents of chemical elements were analyzed by X-ray fluorescence (XRF) at high  
159 resolution (2 mm sampling step) on the surface of the sediment core with an Avaatech core scanner  
160 (EDYTEM Laboratory, CNRS-Université Savoie Mont-Blanc). The core surface was first covered with a  
161 4- $\mu\text{m}$ -thick Ultralene film to avoid contamination and desiccation of the sediment. The element  
162 intensities were expressed in counts per second (cps). Geochemical data were obtained with  
163 different settings according to the elements analyzed. These settings were adjusted to 10 kV and 1.5  
164 mA for 10 s to detect Si, Ca, Al, Fe, Ti, K, Mn, and S. For heavier elements (*i.e.* Sr, Rb, Zr, Br, and Pb),  
165 measurements were performed at 30 kV and 1.0 mA for 40 s.

### 166 *2.5.2 Sedimentary environmental DNA (sedDNA)*

167 To reconstruct the past vegetation dynamic and the nature of herds (*i.e.*, cows, sheep and  
168 goats) by DNA analysis, we sampled 35 slices of 1 to 2-cm thickness covering the whole sediment  
169 core, following the strict laboratory precautions described in Giguet-Covex et al. (2014). Extracellular  
170 DNA was extracted from the sediment, amplified within 8 PCR replicates and sequenced as described  
171 in supplementary materials. The sequence analyses were performed using the Obitools software

172 (<https://git.metabarcoding.org/obitools/obitools/wikis/home>) (Boyer et al., 2016). For mammals, we  
173 only kept sequences with a match >97 % with the sequences in the reference database and removed  
174 all the sequences assigned to hominidae. Results are given in number of positive PCR replicates. For  
175 plants, we only considered sequences with a match >95 % with the sequences in the reference  
176 database. Then, several filtering steps were applied to remove the potential contaminants (see  
177 supplementary materials for more details). The contribution of each taxon and then of vegetation  
178 types were obtained by doing the sum of the number of reads from each replicate and for each  
179 taxon. Then, we log-transformed these numbers ( $\log(N \text{ reads} + 1)$ ) to correct from the exponential  
180 increase of DNA sequences during the PCR amplification. We calculated the taxon contribution from  
181 these log-transformed read numbers.

182

### 183 *2.5.3 Chronology*

184 The chronology of the sediment sequence is based on ten  $^{14}\text{C}$  measurements performed on  
185 terrestrial plant macroremains, as well as on short-lived radionuclide measurements ( $^{210}\text{Pb}$  and  $^{137}\text{Cs}$ ).  
186 AMS (accelerator mass spectrometer) radiocarbon dates were performed by the Poznan Radiocarbon  
187 Laboratory and the Laboratoire de Mesure  $^{14}\text{C}$  (LMC14) ARTEMIS at the CEA (Atomic Energy  
188 Commission) Institute of Saclay. The  $^{14}\text{C}$  ages were calibrated using the IntCal13 calibration curve  
189 (Reimer et al., 2013). Short-lived radionuclides were used to date the most recent sediments. They  
190 were measured on the upper 24 cm of GER15\_P3 gravity core at the Modane Underground  
191 Laboratory (LSM). Measurements were performed by gamma spectrometry, using high-efficiency,  
192 very low-background, well-type Ge detectors (Reyss et al., 1995).  $^{137}\text{Cs}$  was first introduced in the  
193 environment at the end of the 1950s as by-product of atmospheric nuclear weapons tests (maximum  
194 peak at AD 1963 in the Northern Hemisphere). The Chernobyl accident in 1986 also dispersed  $^{137}\text{Cs}$   
195 into the Northern Hemisphere (Appleby et al., 1991).  $^{210}\text{Pb}$  excess activities ( $^{210}\text{Pb}_{\text{ex}}$ ) are calculated in  
196 the sediment as the difference between total  $^{210}\text{Pb}$  (mixing of erosion and atmospheric deposits) and

197  $^{226}\text{Ra}$  activities at each levels (Goldberg, 1963). Then, we used the Constant Flux/Constant  
198 Sedimentation (CFCS) model and the decay of  $^{210}\text{Pb}_{\text{ex}}$  to calculate the mean sedimentation rates. The  
199 uncertainty of sedimentation rates obtained with this method is derived from the standard error of  
200 the linear regression of the CFCS model. The age–depth model for the entire sequence associating  
201 short-lived radionuclides and  $^{14}\text{C}$  was then generated using R software and the R code package ‘Clam’  
202 version 2.2 (Blaauw, 2010).

#### 203 *2.5.4 Estimating erosion*

204 The erosion was estimated from the lake filling considering the volume of each layer of sediment  
205 in the lake, their dry densities, their corresponding sedimentation rate and the surface of the  
206 catchment (5 km<sup>2</sup>), following the method described in Bajard et al. (2017). We estimated the volume  
207 from the surface corresponding to the current higher lake level of the lake (0.05 km<sup>2</sup>) and the depths  
208 in the core, assuming the sediment is equally distributed on the entire surface area of the lake  
209 (Enters et al., 2008). The approximations made on the calculation of the volume are expected to  
210 overestimate the accumulated mass of sediment, because of the higher accumulation in the deepest  
211 part of the lake, where the core was taken. However, the progradation of the delta should cause the  
212 opposite effect and reduce the overestimation. The mass of sediment was then calculated for each  
213 sampled depth, using the dry density. Only the non-carbonate terrigenous mass of the sediments  
214 was considered, using the Non-Carbonate Ignition Residue (NCIR) of the LOI. The terrigenous masses  
215 of each depth were then integrated according to the time, using the age-depth model, and divided by  
216 the surface of the catchment to estimate the erosion rate per unit area.

217

### 218 3. Results

219

220 **3.1 Identification and formation of soils of the catchment**

221 Three main types of pedogenetic processes, *i.e.*, andosolization, podzolization and  
222 colluviation were identified in the catchment of lake Gers (Fig. 2 and Table 1). A complete description  
223 of the soils is presented in supplement material.

224 Cambisols (GERS1, GERS2, GERS11 and GERS5) present mainly a succession of different  
225 brown horizons. They are characterized by low pH increasing with depth and decreasing OM content  
226 (Fig. 2 and Table 1). Andosols as GERS8 present a darker color due to high OM content throughout  
227 the profile and their pH is low (Fig. 2). They develop on Taveyannaz sandstones which are made of 80  
228 % of volcanic materials (Martini, 1966) that make possible the andosolization in this area. They also  
229 displays the lowest  $K_2O/TiO_2$  ratio (Table1). Podzols as GERS6, GERS7, GERS9 and GERS10 are  
230 characterized by low pH and decreasing OM content in the profile. Colluviation is characterized by  
231 lots of coarse elements, higher pH and low OM contents (GERS3, GERS4 and GERS11 in Fig. 2). These  
232 soils also display the highest  $K_2O/TiO_2$  ratios (Table1).

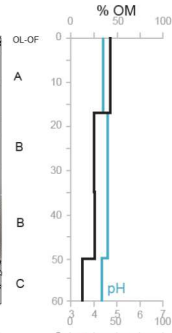
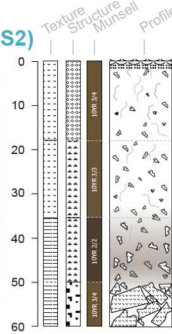
233

234 **[insert FIGURE 2]**

**ANDOSOLIZATION**

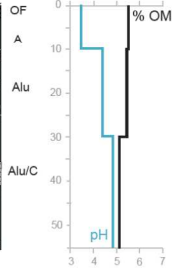
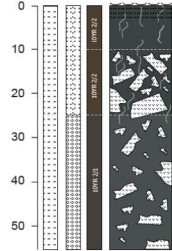
**Andic Cambisols (GERS1 and GERS2)**

**GERS2**  
 46° 0'43,60"N  
 6°43'1,50"E  
 2085 m  
*Vaccinium*



**Andosols**

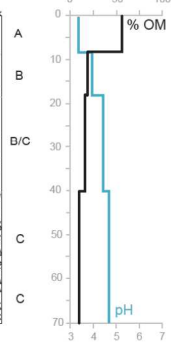
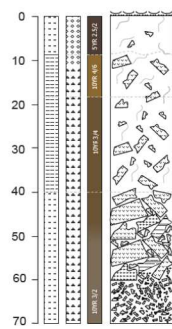
**GERS8**  
 46° 0'0'46,1" N  
 6°44'7,7" E  
 2016 m  
*Vaccinium*



**PODZOLIZATION**

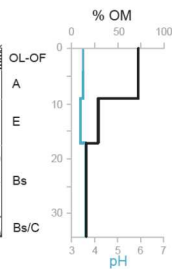
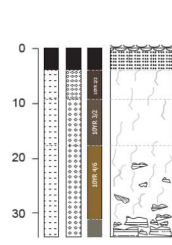
**Cambisols (GERS5) to Entic Podzols (GERS6, GERS7, GERS10)**

**GERS6**  
 46° 0'45,00"N  
 6°43'35,40"E  
 1880 m  
*Alder*



**Podzols**

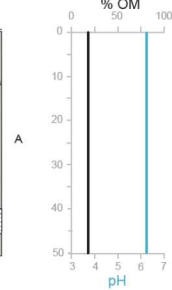
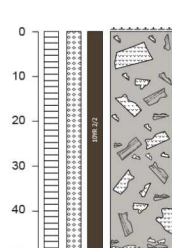
**GERS9**  
 46° 1'16,20"N  
 6°44'23,20"E  
 1990 m  
*Matgrass*



**COLLUVIATION**

**Colluvic Regosols (GERS3, GERS4) and Colluvic Cambisols (GERS11)**

**GERS11**  
 46° 1'40,60"N  
 6°44'39,80"E  
 1573 m



**Legend**

**Texture**

- Silty Loam
- Clay Loam
- Silty Clay

**Structure**

- Lumpy
- Subangular blocky
- Blocky
- Smeary

**Artefacts**

**Coarse elements**

- Taveyannaz sandstone with decarbonation halo
- Marly carbonated facies within Taveyannaz sandstone

**Roots : fine, medium, coarse**

235

236 [insert TABLE 1]

237

238 **TABLE 1. Soil horizon analyses**

Sample	Top depth (cm)	Bottom depth (cm)	Horizon	pH <sub>water</sub>	Bulk density	OM % (LOI 550°C)	Al <sub>2</sub> O <sub>3</sub> %	SiO <sub>2</sub> %	K <sub>2</sub> O %	CaO %	TiO <sub>2</sub> %	MnO %	Fe <sub>2</sub> O <sub>3</sub> %	Zr %	Total %	K <sub>2</sub> O/TiO <sub>2</sub>	
<b>GERS1</b>																	
GERS 1-1	1-1	0	17	A	4.0	0.5	57.0	7.62	23.85	1.07	0.62	1.03	0.08	7.75	0.03	99.1	1.0
GERS 1-2	1-2	17	45	B	4.2	-	26.2	18.31	38.39	1.79	1.18	1.49	0.15	11.29	0.04	98.9	1.2
GERS 1-3	1-3	45	65+	C	5.0	-	7.8	19.65	57.04	2.28	2.31	1.12	0.10	9.10	0.04	99.5	2.0
<b>GERS2</b>																	
GERS 2-1	2-1	0	17	A	4.4	-	43.3	10.71	32.34	1.31	0.80	1.10	0.17	9.44	0.04	99.2	1.2
GERS 2-2	2-2	17	35	B	4.6	-	25.1	16.51	41.95	1.65	1.20	1.36	0.22	11.15	0.04	99.2	1.2
GERS 2-3	2-3	35	50	B	4.6	-	25.8	20.44	38.27	1.71	1.86	1.18	0.13	9.77	0.05	99.2	1.5
GERS 2-4	2-4	50	60+	C	4.3	-	13.0	22.03	48.87	2.26	3.00	1.08	0.10	9.19	0.04	99.6	2.1
<b>GERS4</b>																	
GERS 4-1	4-1	0	20	A/C	6.1	-	17.1	15.54	50.99	3.12	2.58	0.84	0.18	8.01	0.03	98.4	3.7
GERS 4-2	4-2	0	10	A/C	6.7	-	11.9	16.57	53.78	3.44	2.57	0.88	0.20	8.45	0.04	97.8	3.9
<b>GERS5</b>																	
GERS 5-1	5-1	0	15	A	4.1	0.8	28.0	13.55	45.46	2.42	0.55	1.01	0.09	8.11	0.04	99.3	2.4
GERS 5-2	5-2	15	45+	B/C	4.5	-	13.8	18.15	52.02	2.93	0.72	1.14	0.12	9.00	0.04	98.0	2.6
<b>GERS6</b>																	
GERS 6-1	6-1	0	8	A	3.3	-	55.7	5.99	29.17	1.21	0.60	0.90	0.03	5.64	0.05	99.3	1.3
GERS 6-2	6-2	8	18	B	3.9	-	18.5	15.19	51.45	2.34	0.19	1.37	0.14	10.32	0.06	99.6	1.7
GERS 6-3	6-3	18	40	B/C	4.4	-	16.0	15.19	51.48	3.15	0.13	1.67	0.24	11.76	0.09	99.8	1.9
GERS 6-4	6-4	40	70+	C	4.7	-	9.5	21.86	53.26	3.15	0.66	1.06	0.14	8.63	0.04	98.3	3.0
<b>GERS7</b>																	
GERS 7-1	7-1	0	5	OH	3.3	-	87.2	0.00	7.60	0.18	2.48	0.38	0.00	1.87	0.02	99.7	0.5
GERS 7-2	7-2	5	10	A	3.5	-	25.8	12.03	46.73	1.76	0.85	1.27	0.07	11.13	0.04	99.6	1.4
GERS 7-3	7-3	10	25	B	3.8	-	18.8	17.54	46.53	2.00	0.97	1.35	0.13	10.35	0.05	97.7	1.5
GERS 7-4	7-4	25	50+	C	4.3	-	15.3	18.17	51.31	2.11	1.05	1.23	0.15	10.06	0.04	99.5	1.7
<b>GERS8</b>																	
GERS 8-1	8-1	3	10	A	3.5	0.3	62.5	4.91	21.73	0.76	0.80	1.28	0.02	7.43	0.04	99.5	0.6
GERS 8-2	8-2	10	30	Alu	4.4	-	60.1	10.23	13.82	0.57	0.72	1.03	0.10	12.56	0.03	99.2	0.6
GERS 8-3	8-3	30	55+	Alu/C	4.9	0.4	52.5	13.57	18.34	0.66	1.10	0.98	0.18	11.64	0.03	99.0	0.7
<b>GERS9</b>																	
GERS 9-1	9-1	4	9	A	3.5	-	72.2	3.40	18.91	0.89	0.38	0.51	0.02	2.78	0.04	99.1	1.7
GERS 9-2	9-2	9	17	E	3.4	0.6	28.5	10.22	50.51	2.19	0.07	1.27	0.02	5.60	0.07	98.5	1.7
GERS 9-3	9-3	17	31	Bs	3.6	0.7	16.0	16.47	51.66	2.99	0.13	1.04	0.06	8.89	0.03	97.3	2.9
GERS 11	<b>GERS11</b>	0	50+	A	6.2	-	19.7	12.65	51.42	3.01	4.39	0.86	0.13	7.38	0.04	99.6	3.5

239

240 The PCA performed on the geochemistry of both the rocks and soils samples allowed to  
 241 better understand the soil formation and identify different geochemical sediment sources (Fig. 3).

242 Dimensions 1 and 2 (denoted as *Dim 1* and *Dim 2*) of the PCA from the geochemical data of  
 243 the parent materials represent 75.6 % of the total variability (Fig. 3a). Three end members were  
 244 identified on the correlation circle. The first one includes TiO<sub>2</sub> as well as Fe<sub>2</sub>O<sub>3</sub> and SiO<sub>2</sub> and is  
 245 positively correlated with the first dimension of the PCA. It concerns rocks from GERS1, GERS2 and  
 246 GERS8 (Fig. 3a). Al<sub>2</sub>O<sub>3</sub> forms a single end member, positively correlated with the second component  
 247 of the PCA. This second end member contains the parent materials of GERS5, GERS6 and GERS9. The  
 248 third one is negatively correlated with both components and give positive loading between K<sub>2</sub>O and  
 249 CaO. This third end member contains the rocks sample of GERS3 and GERS4. Parent materials of  
 250 GERS11 is located between these three end-members (Fig. 3a).

251 The PCA performed with soil samples includes the same geochemical elements than the rock  
 252 sample PCA ( $\text{SiO}_2$ ,  $\text{Al}_2\text{O}_3$ ,  $\text{TiO}_2$ ,  $\text{Fe}_2\text{O}_3$ ,  $\text{CaO}$ ) and the OM content (Fig. 3b). Dimensions 1 and 2  
 253 represent 78 % of the total variability of this dataset. Dimension 1 gives positive loading to  $\text{Fe}_2\text{O}_3$  and  
 254 negative loadings to  $\text{K}_2\text{O}$ .  $\text{TiO}_2$  and the OM content are correlated to both dimensions. Dimension 2  
 255 (Dim 2) gives negative loading to  $\text{Al}_2\text{O}_3$  and  $\text{CaO}$  but  $\text{CaO}$  is poorly representative in the soil dataset  
 256 (Fig. 3b).  $\text{SiO}_2$  is positively correlated to Dim 2 and negatively to Dim 1. Surface horizons are  
 257 associated with OM direction and conversely, the deepest horizons are anticorrelated to OM.  
 258 Samples from GERS9, GERS6 and GERS5 are mainly associated with Dim 2 and form a “Podzolic”  
 259 endmember. GERS4 and GERS11 are anticorrelated to Dim 1 and closely associated to  $\text{K}_2\text{O}$  (Fig. 3b).  
 260 They form an end-member of low weathered soils, with the deepest horizons of other soils. GERS1,  
 261 GERS2 and GERS8 appear to be mainly associated to  $\text{Fe}_2\text{O}_3$  and  $\text{Al}_2\text{O}_3$  and form an “Andic”  
 262 endmember. GERS7 is in the center of the PCA.

263 [insert FIGURE 3]

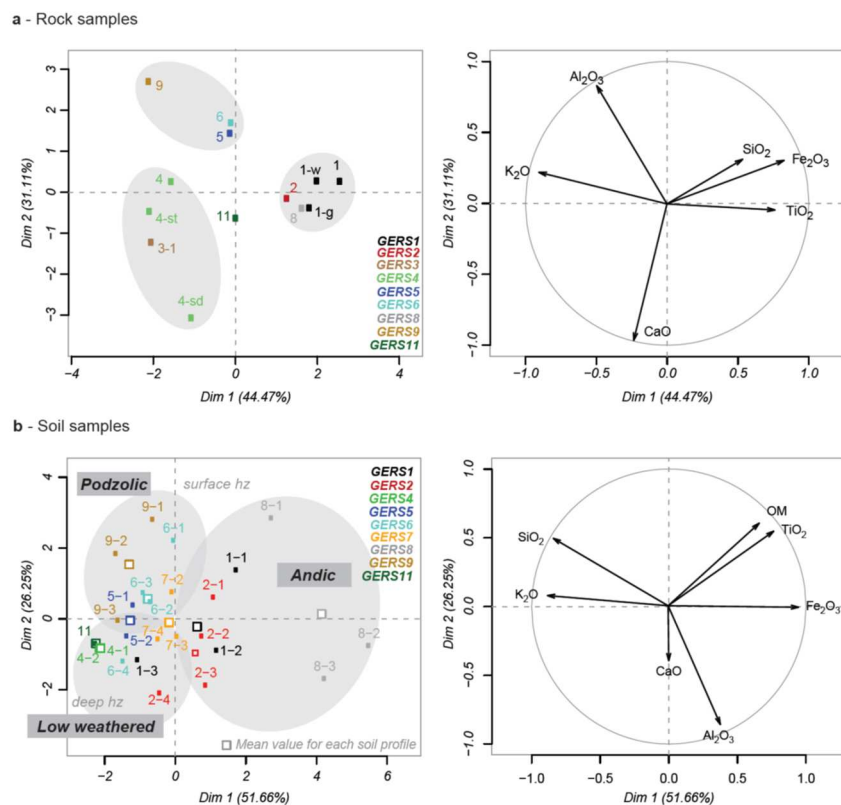


Figure 3. Biplots of dimensions 1 and 2 and correlation circles of the principal component analysis realized with the rock-parent material of soils (a) and with the soil horizon samples (b).

264

## 265 3.2 Core description and lithology

266 The continuous sedimentation of the 5.8 m of the sequence consists mainly of dark medium  
267 silts, with a higher variability between 3 and 1.25 m. The organic matter content is 11 % in average  
268 and the carbonate content is 3 % in average.

269 The sedimentary sequence is interrupted by 127 individual layers that are interpreted as  
270 short-term depositional events according to Sturm and Matter (1978) and Arnaud et al. (2002). 93 of  
271 these deposits are darker graded beds with a coarse and no erosive base and present thicknesses  
272 ranging from the millimeter to the dozens of centimeters. The thickest deposits occur at 5.20 m (12  
273 cm), 3.90 m (9.5 cm), 3.02 m, (13.5 cm), 1.73 m (6.5 cm) and 1.31 m (11 cm). Between 1.80 and 2.00  
274 m, deposits are thinner and more numerous (approximately 30 between 2 and 8 mm of thickness).

275 The 34 other deposits are very fine sand layers from less than 1 mm to 5 mm, located only in  
276 the bottom part of the core, between 4.8 and 5.8 m.

277 A more complete description of the sediment analyses according to depth is presented in the  
278 supplementary materials.

## 279 3.3 Age-depth model and instantaneous deposits

### 280 3.3.1 Short-lived radionuclides

281 The measurement of short-lived radionuclides allowed the dating of the uppermost 16 cm of  
282 the core. A logarithmic plot of  $^{210}\text{Pb}_{\text{ex}}$  activity (Fig. 4a) shows a downward decrease from the surface.  
283 The three deepest points measured were rejected because of their distance from the main  
284 logarithmic trend (reach the secular equilibrium). In the same way, the  $^{210}\text{Pb}_{\text{ex}}$  measures realized in  
285 the 9.6-12.5 cm and 12.5-15.5 cm deposits present lower activities and were excluded from the  
286 construction of an event-free sedimentary record because they were considered as instantaneous  
287 deposits (Arnaud et al., 2002). The depth-corrected plot of  $^{210}\text{Pb}_{\text{ex}}$  activities (*i.e.* depth without  
288 instantaneous events) shows two logarithmic relationships providing two mean sedimentation rates:  
289  $2.9 \pm 0.5 \text{ mm.yr}^{-1}$  above 5 cm and  $1.3 \pm 0.2 \text{ mm.yr}^{-1}$  below. Ages were then calculated using the

290 'constant flux, constant sedimentation rate' (CFCS) model (Goldberg, 1963; Krishnaswamy et al.,  
 291 1971) applied to the original sediment depth to provide a continuous age-depth relationship.

292 The <sup>137</sup>Cs activity profile (Fig. 4a) has a peak beginning at a depth of 16.5 ± 0.25 cm and  
 293 reaches a maximum at 13.5 ± 0.25 cm, interpreted respectively as the beginning of atmospheric  
 294 production of <sup>137</sup>Cs, in AD 1955 due to nuclear weapon test in the Northern Hemisphere and its  
 295 maximum fallout in AD 1963 (Robbins and Edgington, 1975). The good agreement between the ages  
 296 of the beginning and maximum artificial radionuclide fallout inferred from the <sup>210</sup>Pbex-CFCS model  
 297 (1952 and 1965) and their known ages (1955 and 1963) supports the validity and the accuracy of our  
 298 age-depth model in the upper 16 cm of the sediment sequence.

### 299 *3.3.2 Radiocarbon dating*

300 A total of 10 radiocarbon analyses were performed on selected macrofossils collected from  
 301 the 5.8-m length of the sediment core (Table 2). These data and those from the short-lived  
 302 radionuclides measurements were incorporated into Clam to generate the age–depth model of the  
 303 whole core (Fig. 4b). SacA42472 sample appear too old. It was taken only a few millimeters from an  
 304 instantaneous deposit. Macrofossils had thus probably been reworked, explaining the age obtained.  
 305 In consequence, this radiocarbon date was not considered for age–depth modeling. Nevertheless, its  
 306 high uncertainty, due to its young age, stays in the smooth model computed (Fig. 4b).

307 **[insert TABLE 2]**

Table 2. Radiocarbon ages for Lake Gers sediment sequence

Sample name	Lab. Code	Depth (mm)	Sample type	Age (yr BP)	Min. age (cal yr BP)	Max. age (cal yr BP)
<b>GER1</b>	<b>SacA42472</b>	<b>465</b>	<b>Herbs, seeds</b>	<b>315 ± 30</b>	<b>303</b>	<b>463</b>
GER2	SacA42473	1155	Herbs	620 ± 30	552	657
GER3	SacA42474	2180	Bark, herbs	1125 ± 30	960	1172

GER16-1	Poz-81888	2395	Herbs, moss, twigs	1345 ± 30	1186	1308
GER16-2	Poz-81889	2862	Bark, twigs	1885 ± 30	1733	1888
GER16-3	Poz-81890	3347	Wood, bark	2145 ± 30	2009	2303
GER16-4	Poz-81891	3911	Wood, bark	2475 ± 30	2382	2719
GER16-5	Poz-81892	4576	Bark	3270 ± 30	3411	3570
GER16-6	Poz-81894	5206	Twigs, herbs, bark, leaves	3830 ± 35	4100	4405
GER16-7	Poz-81895	5706	Herbs, twigs, bark	4020 ± 35	4418	4570

---

**Bold samples correspond to excluded dates from age-depth modeling.**

308

309           The 127 deposits interpreted as instantaneous events represent a total of 163 cm that were  
310 removed from the main continuous sedimentation. The remaining 4.2 m of sediment were used to  
311 build an event-free sedimentary record (Bøe et al., 2006; Wilhelm et al., 2012). We then calculated  
312 an age-depth relationship by a smooth spline interpolation (Fig. 4c). This age-depth model was used  
313 to date all instantaneous deposits.

314 **[insert FIGURE 4 – Age model]**

315           The 5.8 m of sedimentary sequence cover the last 4.6 kyr. The sedimentation varies from 0.5  
316 to 2 mm.yr<sup>-1</sup> with maxima between 4.6 and 4.3 cal kyr BP (1.2 mm.yr<sup>-1</sup>), 2.5 and 1.9 cal kyr BP (1  
317 mm.yr<sup>-1</sup>), 900 and 500 cal yr BP (1.7 mm.yr<sup>-1</sup>) and over the last century (2 mm.yr<sup>-1</sup>).

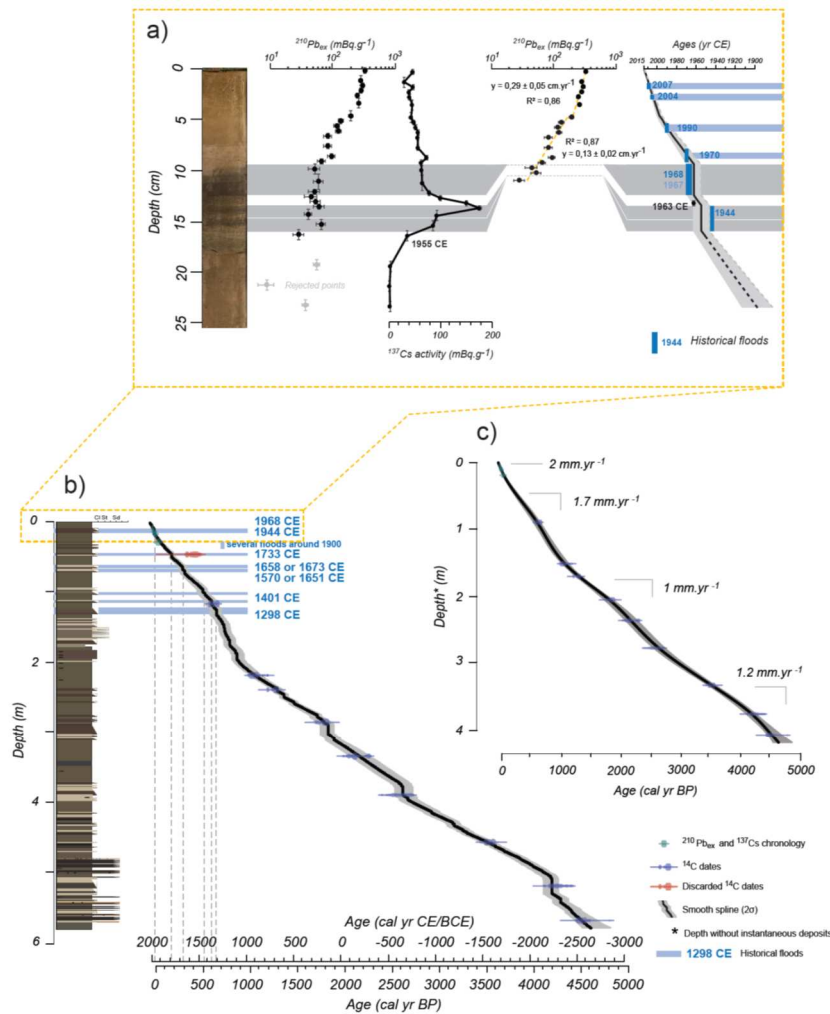


**Figure 4.** Age-depth model of Lake Gers sediment sequence including  $^{210}\text{Pb}$ / $^{137}\text{Cs}$  chronology (a) and  $^{14}\text{C}$  ages (b). Uncertainties are included in the  $^{137}\text{Cs}$  activity dots. (c) corresponds to the continuous age-depth model, without instantaneous deposits. Historical floods were collected from Mougín (1914) for the Giffre valley, from RTM online database (<http://rtrm-onf.ifn.fr>) and from municipal documents. CE= Common Era, BCE= Before Common Era.

318

### 319 3.4 Sedimentary DNA

320 DNA analysis were performed only in the continuous sedimentation to avoid possible  
 321 taphonomic biases especially due to grain-size effects that might occurred in instantaneous deposits.  
 322 Extracellular DNA is expected to be more concentrated in the clayey part than in the sandy/coarse  
 323 silts part of the flood deposit (Giguët-covex et al., 2019).

324 The DNA of six mammalian taxa was detected in the sediments of Lake Gers, specifically *Bos*  
 325 sp. (cattle), *Canis* sp. (dog/wolf), *Capra* sp. (goat), *Felis* sp. (cat), *Ovis* sp. (sheep) and *Sus* sp. (pig). We  
 326 only focus on the three taxa associated with grazing activities: *Bos* sp. *Ovis* sp. and *Capra* sp. (Fig. 5a).  
 327 *Bos* sp. was detected in two samples at 2000 and 1750 cal yr BP, but in only one replicate over eight.  
 328 It was then recorded in all samples younger than 850 cal yr BP, except in the youngest sample. The

329 highest number of positive PCR replicates was measured at 850, 700 and 400 cal yr BP (3, 6 and 4  
330 positive PCR replicates over 8, respectively, Figure 5a). *Ovis* DNA was detected in the two samples  
331 between 850 and 800 cal yr BP (4 and 5 positive replicates over 8) and in the two samples between  
332 700 and 550 cal yr BP (2 and 1 replicates). *Capra* DNA was detected in two samples between 850 and  
333 750 cal yr BP in 1 or 2 PCR replicates and in the two samples between 400 and 200 cal yr BP in 1 PCR  
334 replicates each (Fig. 5a).

335 For the plants, after the filtering steps, 99 taxa (MOTU) were obtained and classified  
336 according to the vegetation stratification and types (*i.e.*, tree layer, shrub layer, herbaceous layer,  
337 moss and ferns). We only present in Figure 5b the tree layer which includes *Prunus*, *Maleae*,  
338 *Aquifoliaceae*, *Betulaceae*, *Populus*, *Picea*, *Pinaceae*, *Ulmaceae*, *Alnus* and *Acer*. The sample at 4.2 cal  
339 kyr BP was removed from our analysis because it contained only 2 taxa detected in 1 or 2 replicates  
340 (*Apioidaeae* and *Polytrichaceae*) any tree sequence, whereas all the other samples older than 1.9 cal  
341 kyr BP contain between 15 and 56 % of tree DNA sequences (32 % in average).

342 From 4.6 to 1.9 cal kyr BP, the DNA of trees represents 31,5% in average, and 13,5% from 1.9  
343 to the present day (Fig. 5b). During this last period we identified a period of higher tree DNA  
344 between 1300 and 900 cal yr BP with 25% in average. The complete sedDNA study combined with  
345 pollen analysis of the Lake Gers sediment sequence has been presented by Blanchet et al. (2019) and  
346 is subject of a publication in preparation.

347

348 **[insert FIGURE 5 – Evolution of landscape]**

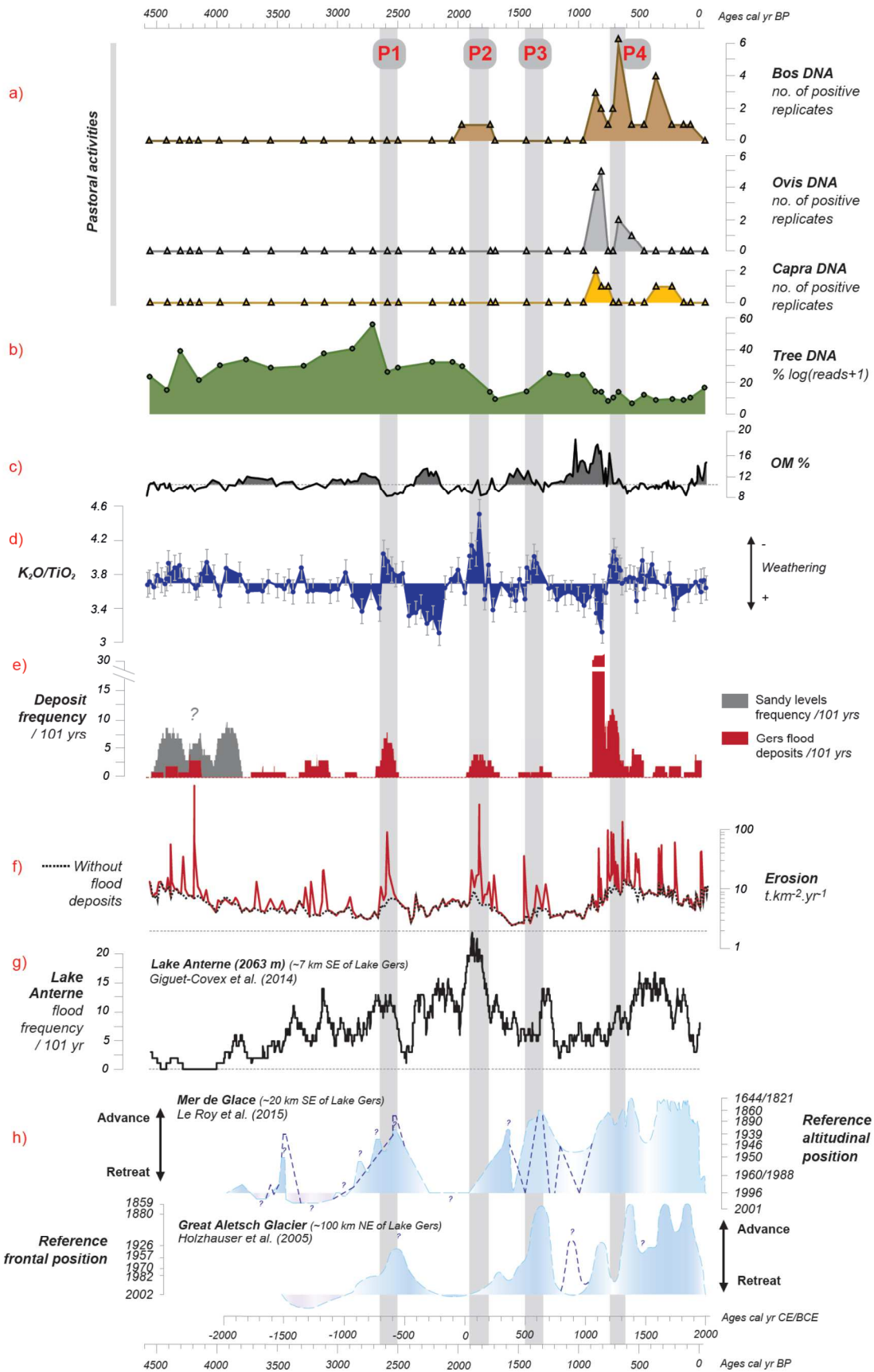


**Figure 5.** Evolution of agro-pastoral activities, vegetation and erosion in the Lake Gers catchment during the late Holocene as inferred from mammal DNA, including DNA of cow, sheep and goat (a), tree DNA (b), organic matter (OM) content (c),  $K_2O/TiO_2$  ratio (d) measured in the continuous sedimentation, the centennial deposit frequency in Lake Gers (e), erosion in Lake Gers catchment (f), compared to Lake Anterne centennial flood frequency (g) and regional glacier records (h) from Le Roy et al. (2015) and Holzhauser et al. (2005) as climate proxys.

## 350 4. Discussion

### 351 4.1 Source-to-sink dynamics

#### 352 4.1.1 Pedological origin

353 PCA for geochemical data from the parent materials (Fig. 3a) highlighted heterogeneity in the  
354 geochemistry of Taveyannaz sandstones, especially between the real sandstones characterized by a  
355 weathering carbonated aureole found in GERS1, GERS2 and GERS8 and the alternating layer of thick  
356 sand and marly levels (GERS3, GERS4). Marly levels were found at lower altitudes than the  
357 Taveyannaz sandstones of GERS1, GERS2 and GERS8 (Fig. 1). Considering its colluvial position,  
358 GERS11 can be feed by both facies (Fig. 1 and 2). The third main parent material can be associated to  
359 glacial deposits in the center (GERS5 and GERS6) and upper part (GERS9) of the catchment (Fig. 1 and  
360 2). PCA from the soil samples defined the same groups as the rock sample PCA, with a distinction for  
361 surface and deep horizons. This scheme reflects a strong relation between parent material and soil  
362 evolution processes in this catchment. GERS1, GERS2 and GERS8 are affected by andic properties,  
363 GERS9, GERS5 GERS6, GERS7 by podzolization and GERS3, GERS4 and GERS11 are low developed and  
364 affected by erosion and colluviation. The development of Andosols is rare in the Alps and no  
365 Andosols has been described in the French Alps to our knowledge. Their development is possible  
366 here from the weathering of Taveyannaz Sandstones which formed from sedimentary deposition of  
367 old eroded volcanic complex.

368 The less weathered soils of Gers catchment, and the deepest soil horizons present high  
369  $K_2O/TiO_2$  ratios (Table 1). In the sediments, increases in  $K_2O/TiO_2$  ratios will represent less weathered  
370 source inputs (young materials, from regular erosion area), or increasingly deep horizons inputs.  
371 Values of  $K_2O/TiO_2$  in the sediments are in the higher range, and beyond what is observed in soils  
372 (Fig. 7d and Table 1). In summary, the main sources of sediment are low weathered soils such as  
373 GERS11 and GERS4.

374 Several phases present high contents of OM when  $K_2O/TiO_2$  ratios, erosion and flood deposit  
 375 frequency are the lowest (Fig. 5). These phases can be interpreted or by slight erosion of soil surface,  
 376 either as the expression of lacustrine OM that is less diluted than during the periods of higher  
 377 terrigenous inputs. Between 900 and 800 cal yr BP, the increase in OM may be also link to grazing on  
 378 the delta of the lake, which could have bring lots of organic matter from dungs.

379

#### 380 4.1.2 Flood chronicle

381 Normally graded deposits are common features in lake sediments. There are commonly  
 382 associated to turbidity currents triggered by mass movements or by flood events. To verify this  
 383 hypothesis, we compared our record with the historical flood calendar of the downstream Giffre  
 384 river established by Mougin (1914) and completed by local archives and internet database of RTM  
 385 (ONF-RTM database, <http://rtm-onf.ifn.fr>). The comparison allows to associate the thickest deposits  
 386 to historical floods from CE 1298 to today (Table 3). The proposed dates fitted within 20 years in  
 387 average, throughout the last 650 years. Only three deposits dated at 513 cal yr BP could not be  
 388 identified in the historical archives, possibly due to both their low thicknesses and their old age  
 389 (Table 3). This good correspondence supports both the assumption of the torrential origin of these  
 390 deposits and the chronology of the sequence for this period.

391

392 **[insert TABLE 3]**

393 **Table 3. Comparison of flood deposits recorded in Lake Gers sediments with historical floods of the Giffre River for the**  
 394 **last 650 yrs. CE= Common Era.**

Flood thickness (cm)	Age cal. BP	Age cal. CE	min CE	max CE	Historical flood	Age difference (yrs)	Reference	Historical document
3	-14	1964	1971	1956	1968	4	RTM archives	
1	-6	1956	1964	1947	1944	12	Municipal archives (Sixt-Fer à Cheval)	
1	-6	1959	1964	1947	1944	12	Municipal archives (Sixt-Fer à Cheval)	

0.5	79	1871	1890	1856	1878	7	Mougin (1914)	Patriote Savoisien, 1878, 2 juin, 21 juin, 4 septembre
1.5	204	1746	1776	1716	1733	13	Mougin (1914)	Arch. Dép. H.-S. T. P. Fy. Liasses anciennes, 14 juin 1737, n°236
2.5	204	1746	1776	1716	1733	13	Mougin (1914)	Arch. Dép. H.-S. T. P. Fy. Liasses anciennes, 14 juin 1737, n°236
3.5	318	1632	1672	1593	1658 or 1673	26 or 41	Mougin (1914)	Revue savoisienne, 1898. Gonthier. Eboulements historiques.
3.5	338	1612	1654	1572	1570 or 1651	46 or 39	Mougin (1914)	Revue savoisienne, 1898. Gonthier. Eboulements historiques.
1	513	1437	1490	1390	?	-	-	
1	513	1437	1490	1390	?	-	-	
1	513	1437	1490	1390	?	-	-	
2	534	1416	1470	1369	1401 ?	15	Mougin (1914)	Acad. Sallès Tome XX. Abbé Feige. Monographie de Mélan.
5	595	1355	1409	1307	1401 ?	46	Mougin (1914)	Acad. Sallès Tome XX. Abbé Feige. Monographie de Mélan.
11	641	1309	1364	1258	1298	11	Mougin (1914)	Acad. Sallès Tome XX. Abbé Feige. Monographie de Mélan.

395

396 The frequency of the instantaneous deposits was estimated for a period of 101 years (Fig. 5i)

397 (Fig. 5e). Sandy levels are presented in a different color as they can have a different origin from the

398 other events and are only present from 4.6 to 3.8 cal yr BP (Fig. 5e). Sandy levels occur from 2 to 10

399 deposits per 101 years on this period, with three higher frequency periods around 4.4, 4.15 and 3.9

400 cal kyr BP. The frequency of the other deposits ranges from 0 to 33 events (Fig. 5e). The centennial

401 frequency ranges from 0 to 4 between 4.6 and 2.7 cal kyr BP, with up to 4 events from 4.6 to 4.15,

402 3.7 to 3.5, 3.3 to 3.1 and 2.95 to 2.85 cal kyr BP. The frequency reaches 8 events per 101 years

403 between 2.7 and 2.5 cal kyr BP before a period where no events were recorded between 2.5 and

404 1.95 cal kyr BP. The frequency reaches up to 4 events again from 1.95 to 1.65 cal kyr BP and up to 2

405 events between 1.5 and 1.23 cal kyr BP. The maximum frequency occurs from 900 to 670 cal yr BP

406 with up to 33 events between 900 and 800 cal yr BP (Fig. 5e). The frequency stays between 2 and 4

407 events per 101 yrs until 460 cal yr BP, then between 0 and 2 until the last century.

408 The origin of sandy deposits between 4.6 and 3.8 cal kyr BP is not solved. As two of them are

409 associated to a graded layer, a flood deposit is possible, but can also be due to chance, *i.e.*, a sand

410 deposit followed by a flood deposit. No other proxies analyzed in the sediment core provide

411 information about the disappearance of these deposits after 3.8 cal kyr BP. They correspond to  
412 another source which is no longer mobilized or which does not reach the lake since 3.8 kyr. They  
413 happen while very low flood-frequency and erosion are recorded at Lake Anterne (Fig. 5g). 3.8 kyr is  
414 also considered as a major paleohydrological transition toward wetter regional conditions as  
415 evidenced by different studies in the Alps (Nicolussi et al., 2005; Magny et al., 2011; Arnaud et al.,  
416 2012; Le Roy et al., 2015; Arnaud et al., 2016; Rapuc et al., 2019). This change in the sedimentary  
417 dynamic could be a consequence of the 4.2 kyr event recognized in different types of archives at  
418 many global locations. The avalanches that arrive on the lake can also bring sands when ice is  
419 melting, especially from the Taveyannaz sandstones cliff above (Fig. 1c). However, they appear to  
420 have a constant grain-size, while avalanches bring very different grain-size materials (weak sorting),  
421 and usually even coarse (e.g., gravels, pebbles) with dropstones in lake sediments (Fouinat et al.,  
422 2017b).

#### 423 *4.1.3 Long-term erosion*

424 Erosion was first calculated without the instantaneous deposits (Fig. 5f, dotted line), and  
425 then including each instantaneous deposit (Fig. 5f). Erosion is approximately  $10 \text{ t.km}^{-2}.\text{yr}^{-1}$  between  
426 4.6 and 4.1 cal kyr BP, with three highest peaks at 30, 50 and  $200 \text{ t.km}^{-2}.\text{an}^{-1}$  during the years of  
427 instantaneous deposits. Erosion decrease at approximately 4-5 to  $3 \text{ t.km}^{-2}.\text{yr}^{-1}$  from 4.1 to 2.6 cal kyr  
428 BP, with punctual event induced-erosion peaks until  $20 \text{ t.km}^{-2}.\text{an}^{-1}$ . Erosion increases at  $9 \text{ t.km}^{-2}.\text{yr}^{-1}$   
429 between 2.6 and 1.7 cal kyr BP, with two highest periods from 2.6 to 2.5 and 1.9 to 1.7 cal yr BP.  
430 Erosion is lower from 1700 to 950 cal yr BP except during the higher event frequency period from 1.4  
431 to 1.3 cal kyr BP (Fig. 5ef). Erosion increases up to  $15 \text{ t.km}^{-2}.\text{yr}^{-1}$  outside flood deposits and up to  $100$   
432  $\text{t.km}^{-2}.\text{yr}^{-1}$  with flood deposits between 950 and 600 cal yr BP, and slightly decreases from 600 to 0 cal  
433 yr BP. The last 65 yrs are characterized by an increase erosion trend.

434 The calculation of erosion is very simplified and absolute values are to be carefully used.  
435 Nevertheless, they are in the order of magnitude of erosion modeled and recorded in Europe (Enters

436 et al., 2008; Cerdan et al., 2010; Egli et al., 2014; Vanmaercke et al., 2015). Furthermore, Bajard et al.  
437 (2017) showed that the uncertainty of the volume of sediment weakly influenced the amount of  
438 erosion. Otherwise, with instantaneous inputs from floods, the erosion triggered at each of these  
439 deposits is very depending of the deposit time of the considered “sample depth” below. Without  
440 considered the flood inputs, erosion is still higher during higher flood-frequency periods, suggesting  
441 an impact of these events on the continuous sedimentation. For example, a part of the material  
442 mobilized during an extreme event can be stocked in the catchment before being remobilized with  
443 later rainfall. This assumption is strongly supported by the variation of  $K_2O/TiO_2$  that displays always  
444 higher values during high flood-frequency periods (Fig. 5de).

445

#### 446 *4.2 Environmental dynamics and agro-pastoral activities in the late Holocene*

447 In the Northwestern Alps, first important developments of pastures happened after 3600 to  
448 3000 cal yr BP. In the Anterne mountain (Fig. 1e), palynological studies from Survilly and Ecuellas  
449 peat bogs show an expansion of *Alnus* around 3600 and 3000 cal yr BP respectively, and were  
450 associated to clear-cutting and grazing activities (David, 2010a, 2010b). Archaeological evidences  
451 found close to Lake Anterne confirms, with sedDNA from the lake, the long livestock farming history  
452 of this area (Rey, 2008, 2010; Giguet-Covex et al., 2014). Similar observations were made in the Swiss  
453 Alps from Lake Sägitalsee at 1935 m a.s.l. (Wick et al., 2003). It is also during this same period that  
454 first human clearing and grazing activities were identified in the area of the Petit Saint Bernard pass  
455 (2188 m a.s.l, French-Italian border), by independent palynological, DNA, pedoanthracological and  
456 archaeological studies (Talon, 2006; Rey et al., 2008; Bajard et al., 2017b).

457 At lake Gers, the period between 4600 and 2700 cal yr BP is characterized by no or low  
458 variations of the geochemistry with four periods of low flood-frequency, reflecting constant inputs  
459 and slight evolution in the landscape. The catchment was rather forested. No pasture activity was

460 recorded by DNA. At 2700 cal yr BP, the peak in tree DNA (Fig. 5b) is mainly due to *Alnus* (data not  
461 shown). This occurrence of *Alnus*, could reflect first development of grazing in lake Gers catchment.

462 After 2700 cal yr BP, both OM contents and  $K_2O/TiO_2$  ratio present higher variations, mainly  
463 anticorrelated. The four phases of higher  $K_2O/TiO_2$  ratio (noted P1 to P4, Fig. 5), reflecting the  
464 contribution of less weathered materials are associated to higher flood-frequency periods. They  
465 appear as ruptures in the evolution of the landscape. Floods had to disrupt the catchment bringing  
466 less weathered materials from rejuvenated soils through erosion and colluviation movements, while  
467 outside periods of higher flood-frequency, the continuous sedimentation reflected the low erosion of  
468 surface soils, with higher OM contents and higher weathered materials.

469 The Roman period is marked a slight decrease of DNA of trees and the first occurrence of  
470 cow DNA in the sediments between 2000 and 1700 cal yr BP, suggesting deforestation and  
471 development of cattle grazing in the catchment. The rejuvenation of soils between 1900 and 1750 cal  
472 yr BP (P2 phase) is associated with this development of grazing activities. On the other hand, cow and  
473 bos DNA were detected earlier in the sediments of lake Anterne (Fig. 1e), between 2400 and 1900  
474 cal yr BP (Giguët-Covex et al., 2014). This difference could reflect a development of pastoral areas by  
475 the areas at higher altitudes.

476 Between 1300 and 900 cal yr BP, a recovery in the forest restored surface soil inputs. No  
477 flood deposit was recorded during this period. A similar recolonization of the vegetation was  
478 recorded at Lake Verney (2088 m) in the Petit Saint Bernard pass area (French-Italian border),  
479 approximately at the same period with evidence of a slight recovery in the podzolic processes in the  
480 catchment (Bajard et al., 2017b). The origins of this decrease in pastoral activities could therefore be  
481 more global (*e.g.*, climate forcing).

482 After 950 cal yr BP, cattle grazing activities seems to be continuous. Sheep and goat were  
483 present especially until 800 cal yr BP. The Gers valley is known to be one of the main route to bring  
484 animals to the Sales Vallon (Fig. 1e), which is another pasture located a few kilometers away

485 (Guffond and Mélo, 2018). At Sales, 84 archaeological structures and remains of building were  
486 identified (Guffond, 2017). Two animal bones, buried in the buildings, were dated 865 and 675 yr BP.  
487 They independently confirm the medieval implantation of these mountains. Moreover, the  
488 intensification of agricultural activities in this part of the Alps in the medieval period was also  
489 reflected by the expansion and opening of new grazing areas like at Bénit, a pasture located 18 km  
490 west of Gers (Bajard et al., 2018).

491 This diversification of the pastoral activities was associated with the expansion of pastoral  
492 areas, as suggested by the decrease in the DNA of trees and increase in erosion of OM-rich and highly  
493 weathered soils associated with the high frequency of thin flood deposits. They suggest a progressive  
494 erosion of soils, from weathered and organic surface horizons to deep, less weathered horizons (P4  
495 phase), leading to a more important development of Cambisols, instead of Podzols and Andosols.  
496 From 700 cal yr BP to the present, few changes were recorded except the relative decrease in flood-  
497 frequency, suggesting a stabilization of the landscape. Historical documents from 1418 CE (532 yr cal  
498 BP) attests that animals and heifers were bring to Sales Vallon (Guffond and Mélo, 2018). In 1847,  
499 300 cows were grazing below Pointe Pelouse.

#### 500 *4.3 Impact of climate and human in the subalpine area*

##### 501 *4.3.1 Erosion and climate patterns at the local scale*

502 For both the Roman and medieval periods (P2 and P4 phases, Figure 5), the increases in  
503 erosion, flood-frequency and  $K_2O/TiO_2$  ratio appear to be mostly due to human activities. For the two  
504 other periods (P1 and P3 phases), the impact of human activities could be under-recorded, especially  
505 at the early beginning of the deforestation process. Changes in vegetation may be partly masked in  
506 the first hundred years after landscape modifications, as DNA may be stored in soils, and will only be  
507 transferred to the lake with erosion (Parducci et al., 2017; Giguët-covex et al., 2019). The extreme  
508 values of  $K_2O/TiO_2$  ratio and the highest flood-frequency recorded in the same way than during P2  
509 and P4 phases constitute one more argument in the assumption of human induced flood-frequency

510 increase in P1 and P3 phases, considering that roman and medieval periods were the main periods of  
511 pastoral activities in the Alps.

512 In order to verify this hypothesis, we compared the Lake Gers record with regional glacier  
513 records (Fig. 5h). Holzhauser et al. (2005) and Le Roy et al. (2015) provide reconstitutions of the  
514 dynamics of the Great Aletsch Glacier (100 km northeast of Lake Gers) and of the Mer de Glace (20  
515 km southeast of Lake Gers), respectively, throughout the last 3500 yrs. Both P1 and P3 phases are  
516 synchronous with glacier advances of both glaciers, suggesting mainly a climate cooling to explain the  
517 higher flood-frequency periods and the associated erosion increases. Around the Alps, Arnaud et al.  
518 (2016) pointed out that colder periods generally favour higher flood frequency. Indeed, a climate  
519 cooling could affect vegetation by reducing its development. But vegetation protects soils from  
520 erosion, and soils also absorb precipitation, limiting run off and flooding. So, a cooling of the climate  
521 could increase flood events.

522 The P4 phase but also all the last millennia of Lake Gers sedimentary record is also largely  
523 associated to glacier fluctuations. The P4 phase could thus be associated to both climate and human  
524 forcings. Both effects of substantial land-use and precipitation patterns changes could be responsible  
525 for the higher flood-frequency recorded at the beginning of the last millennia.

526 In order to draw the regional pattern of erosion we compared the Lake Gers record with Lake  
527 Anterne sedimentary record (7 km southward). At Anterne, both the flood-frequency and  
528 sedimentation rate, which present the same variations, were used as proxies of erosion (Giguët-  
529 Covex et al., 2011, 2012), as observed in Lake Gers sequence. Higher flood-frequency was recorded  
530 at Lake Anterne (max 24/101 yrs, 7 /101 yrs on average) than at Lake Gers (max 33/101 yrs, 2/101 yrs  
531 in average). The catchment of Lake Anterne is possibly more susceptible to flood because of both its  
532 higher altitude (*e.g.*, difference in vegetation, precipitations and snow melting) and the highest  
533 erodibility of the schists, which mainly cover its catchment. Pastoral activities at Anterne were  
534 recorded mainly from 2400 to 1900 cal yr BP (cow and sheep) and from 1000 to 200 cal yr BP (mainly

535 cow) (Giguët-Covex et al., 2014). The effects of human activities seem to be more marked at Anterne  
536 during the late Iron age and the beginning of roman period, with both cow and sheep grazing,  
537 associated with maximum of erosion, while this period is much more weakly marked by human  
538 activities at Lake Gers (Fig. 5).

539         The erosion recorded in both lakes display similar variations, especially between 3200 and  
540 1000 cal yr BP. After 1000 cal yr BP, both erosion patterns seem more different. At Lake Anterne,  
541 erosion increases slightly, and more after 500 cal yr BP in relation with wetter and colder climate  
542 conditions of the Little Ice Age (Giguët-Covex et al., 2012). At Lake Gers, erosion was very important  
543 after 950 cal yr BP, in relation with human activities, triggering a high destabilization of soils and an  
544 increase of flood deposits. Erosion trajectories of soils in both catchments are similar while human  
545 impact is moderated, as noticed in the Roman period, and then differ when human pressure  
546 strengthens in the Middle Age. This comparison suggests that from the medieval period, human  
547 activities overwhelm the impact of climate on erosion in Lake Gers catchment. A similar observation  
548 was realized from Lake La Thuile sediment sequence for the same period (Bajard et al., 2016). Both  
549 erosion and soil disruption were triggered first by climate forcing (*i.e.*, heavy precipitations, snow  
550 cover duration) and strongly increase according to the intensity of human activities that disrupt soils  
551 and make them more easily erodible. However, changes in hydrological patterns could be more  
552 associated to bare soils than change in vegetation (Cosandey et al., 2005). Such an increase in the  
553 erodibility of a catchment with anthropic activities was also recorded in the southern Alps and  
554 represent a major threat for the future (Brisset et al., 2017).

#### 555 *4.3.2. Consequences of land use modifications on the vulnerability to climate changes*

556         Long-term changes in land use has led to an increase in transport capacity of water in the  
557 catchment (*e.g.* increased of Hortonian flow due to vegetation changes or compaction) and increase  
558 in the sediment supply through the erosion initiated by grazing activities and deforestation. These  
559 consequences triggers an input of water and sediments more important to downstream areas where

560 human activities take place. In interaction with climate changes and multiplication of extreme  
561 events, these consequences increase the vulnerability of population to flood hazards. Therefore,  
562 upstream areas should be more taken into account in the adaptation to climate change and risk  
563 prevention plans.

564           Effect of floods, favored by human-induced land-use changes increases losses of soils and  
565 their associated ecosystem services. Anthropogenic land-use changes are known to be an important  
566 way to lose organic carbon (Carcaillet et al., 2002; Kaplan et al., 2011). However, human activities  
567 induced-erosion is not well considered in the assessment of organic C losses and in the global C  
568 budget (Lal, 2003). Erosion could yet accelerate organic C losses in the atmosphere, by mineralization  
569 to CO<sub>2</sub>, and strengthen climate warming (Alewell et al., 2009; Wang et al., 2017). The less important  
570 OM content in the sediment of Lake Gers (10 % in average) than in soils of the catchment (30 % in  
571 average, Table 1) suggests a loss of organic carbon with erosion. However, our data do not allow to  
572 assess the location of mineralization, during transport or within the lake. As a result, a larger  
573 consideration and management of upstream areas would reduce the vulnerability of population  
574 downstream to flood events and participate to carbon storage to limit the global warming.

575

## 576       5. Conclusions

577           The sediment sequence of Lake Gers (1540 m a.s.l.) in the Northern French Alps provides a  
578 continuous record of environmental changes throughout the last 4.6 kyr. The sequence is punctuated  
579 by 127 instantaneous deposits, including 93 graded deposits identified as flood deposits. The other  
580 deposits are sand layers occurring only from 4.6 to 3.8 cal kyr BP, whose origin was not determined.  
581 Multiproxy analyses of the continuous sedimentation, including geochemistry, loss on ignition and  
582 DNA analyses, was compared to flood-frequency and to current soils of the catchment. Erosion was

583 quantified from the lake filling, including flood events and compared to regional climate and erosion  
584 records.

585 Three potential geochemical sources were identified in the catchment, corresponding to  
586 variations in geological formations over which different pedogenetic processes were associated, *i.e.*,  
587 Podzolization, Andosolization and colluviation. Colluviation and low weathered material seem to be  
588 responsible for the main inputs in the lake. Podzols and Andosols features were not identified in the  
589 sediment with our analyses.

590 Four phases of decrease in the weathering of sedimentary inputs were associated to higher  
591 flood-frequency periods, suggesting the progressive erosion of soils and their periodic destabilization  
592 and rejuvenation. Two of the four weathering decrease phases (*i.e.* increase in  $K_2O/TiO_2$  ratio) were  
593 associated with climate cooling in the 2650-2500 and 1450-1300 cal yr BP periods. The two other  
594 phases were associated with human activities, *i.e.* deforestation and pastoralism, during the late  
595 Roman period and in the Middle Age, mainly with cow grazing. In the last millennia, agricultural  
596 activities are diversified with sheep and goats, and combined to climate forcing. Both effect,  
597 agriculture and climate, triggered an even higher flood-frequency deposit and higher erosion. This  
598 last anthropic phase evidenced higher modifications operated by agro-pastoral activities in the  
599 catchment (*e.g.*, vegetation) and a higher sensibility to climate events.

600

## 601 6. Acknowledgments

602 The authors thank the municipality of Samoens for access and coring authorizations to Lake  
603 Gers, and the ski resort of Flaine - Grand Massif for the winter access to the lake by the ski slopes  
604 (Malvina Sculo, ski patrols and snow groomer driver). Thanks to Jim Félix-Faure, Laurent Fouinat and  
605 Anouk Leloup-Besson for field support and Dominique Navillod for her welcome to the “Gite de  
606 Gers”. Thanks also to Sarah Bureau for ICP-AES analyses at ISTERRE laboratory. 14C analyses were

607 acquired thanks to the CNRS-INSU ARTEMIS national radiocarbon AMS measurement program at  
608 Laboratoire de Mesure du 14C (LMC14) in the CEA Institute at Saclay (French Atomic Energy  
609 Commission). The authors thank also the Laboratoire Souterrain de Modane (LSM) facilities for the  
610 gamma spectrometry measurements. DNA analyses were supported by AGIR-PAGE Euromont 2016  
611 project. We thank Morgan T. Jones for correcting the English of the article and the two anonymous  
612 reviewers for advice in improving our manuscript.

## 613 7. Data availability

614 Datasets related to this article can be found at  
615 <https://data.mendeley.com/datasets/j9x7yhcvd4/draft?a=1fbbfa5b-b76e-4d5b-b428-adc496d7c2d4>,  
616 (doi:10.17632/j9x7yhcvd4.1) an open-source online data repository hosted at Mendeley Data  
617 ([CITATION TO DATASET]).

## 618 8. References

619

- 620 Adhikari, K., Hartemink, A.E., 2016. Linking soils to ecosystem services — A global review. *Geoderma*  
621 262, 101–111. <https://doi.org/10.1016/j.geoderma.2015.08.009>
- 622 Alewell, C., Schaub, M., Conen, F., 2009. A method to detect soil carbon degradation during soil  
623 erosion. *Biogeosciences Discussions* 6, 5771–5787. <https://doi.org/10.5194/bgd-6-5771-2009>
- 624 Appleby, P., Richardson, N., Nolan, P., 1991. 241Am dating of lake sediments, in: *Environmental*  
625 *History and Palaeolimnology*. Springer, pp. 35–42.
- 626 Arnaud, F., Lignier, V., Revel, M., Desmet, M., Beck, C., Pourchet, M., Charlet, F., Trentesaux, A.,  
627 Tribouvillard, N., 2002. Flood and earthquake disturbance of 210Pb geochronology (Lake  
628 Anterne, NW Alps). *Terra Nova* 14, 225–232.
- 629 Arnaud, F., Poulénard, J., Giguët-Covex, C., Wilhelm, B., Révillon, S., Jenny, J.-P., Revel, M., Enters, D.,  
630 Bajard, M., Fouinat, L., others, 2016. Erosion under climate and human pressures: An alpine  
631 lake sediment perspective. *Quaternary Science Reviews* 152, 1–18.
- 632 Arnaud, F., Révillon, S., Debret, M., Revel, M., Chapron, E., Jacob, J., Giguët-Covex, C., Poulénard, J.,  
633 Magny, M., 2012. Lake Bourget regional erosion patterns reconstruction reveals Holocene  
634 NW European Alps soil evolution and paleohydrology. *Quaternary Science Reviews* 51, 81–  
635 92. <https://doi.org/10.1016/j.quascirev.2012.07.025>
- 636 Bailey, R.W., Becraft, R.J., Forsling, C.L., 1934. *Floods and accelerated erosion in northern Utah*. US  
637 Government Printing Office.
- 638 Bajard, M., Etienne, D., Quinsac, S., Dambrine, E., Sabatier, P., Frossard, V., Gaillard, J., Develle, A.-L.,  
639 Poulénard, J., Arnaud, F., Dorioz, J.-M., 2018. Legacy of early anthropogenic effects on recent

640 lake eutrophication (Lake Bénit, northern French Alps). *Anthropocene* 24, 72–87.  
641 <https://doi.org/10.1016/j.ancene.2018.11.005>

642 Bajard, M., Poulénard, J., Sabatier, P., Develle, A.-L., Giguët-Covex, C., Jacob, J., Crouzet, C., David, F.,  
643 Pignol, C., Arnaud, F., 2017a. Progressive and regressive soil evolution phases in the  
644 Anthropocene. *CATENA* 150, 39–52. <https://doi.org/10.1016/j.catena.2016.11.001>

645 Bajard, M., Poulénard, J., Sabatier, P., Etienne, D., Ficetola, F., Chen, W., Gielly, L., Taberlet, P.,  
646 Develle, A.-L., Rey, P.-J., Moulin, B., Beaulieu, J.-L. de, Arnaud, F., 2017b. Long-term changes  
647 in alpine pedogenetic processes: Effect of millennial agro-pastoralism activities (French-  
648 Italian Alps). *Geoderma* 306, 217–236. <http://dx.doi.org/10.1016/j.geoderma.2017.07.005>

649 Bajard, M., Sabatier, P., David, F., Develle, A.-L., Reyss, J.-L., Fanget, B., Malet, E., Arnaud, D.,  
650 Augustin, L., Crouzet, C., Poulénard, J., Arnaud, F., 2016. Erosion record in Lake La Thuile  
651 sediments (Prealps, France): Evidence of montane landscape dynamics throughout the  
652 Holocene. *The Holocene* 26, 350–364.

653 Blaauw, M., 2010. Methods and code for ‘classical’ age-modelling of radiocarbon sequences.  
654 *Quaternary Geochronology* 5, 512–518. <https://doi.org/10.1016/j.quageo.2010.01.002>

655 Bøe, A.-G., Dahl, S.O., Lie, Ø., Nesje, A., 2006. Holocene river floods in the upper Glomma catchment,  
656 southern Norway: a high-resolution multiproxy record from lacustrine sediments. *The*  
657 *Holocene* 16, 445–455. <https://doi.org/10.1191/0959683606hl940rp>

658 Boyer, F., Mercier, C., Bonin, A., Le Bras, Y., Taberlet, P., Coissac, E., 2016. obitools: a unix-inspired  
659 software package for DNA metabarcoding. *Molecular Ecology Resources* 16, 176–182.

660 Brisset, E., Guiter, F., Miramont, C., Troussier, T., Sabatier, P., Poher, Y., Cartier, R., Arnaud, F., Malet,  
661 E., Anthony, E.J., 2017. The overlooked human influence in historic and prehistoric floods in  
662 the European Alps. *Geology* 45, 347–350. <https://doi.org/10.1130/G38498.1>

663 Carcaillet, C., Almquist, H., Asnong, H., Bradshaw, R., Carrion, J., Gaillard, M.-J., Gajewski, K., Haas, J.,  
664 Haberle, S., Hadorn, P., others, 2002. Holocene biomass burning and global dynamics of the  
665 carbon cycle. *Chemosphere* 49, 845–863.

666 Cerdan, O., Govers, G., Le Bissonnais, Y., Van Oost, K., Poesen, J., Saby, N., Gobin, A., Vacca, A.,  
667 Quinton, J., Auerswald, K., Klik, A., Kwaad, F.J.P.M., Raclot, D., Ionita, I., Rejman, J., Rousseva,  
668 S., Muxart, T., Roxo, M.J., Dostal, T., 2010. Rates and spatial variations of soil erosion in  
669 Europe: A study based on erosion plot data. *Geomorphology* 122, 167–177.  
670 <https://doi.org/10.1016/j.geomorph.2010.06.011>

671 Cosandey, C., Andréassian, V., Martin, C., Didon-Lescot, J.F., Lavabre, J., Folton, N., Mathys, N.,  
672 Richard, D., 2005. The hydrological impact of the mediterranean forest: a review of French  
673 research. *Journal of Hydrology* 301, 235–249. <https://doi.org/10.1016/j.jhydrol.2004.06.040>

674 Daily, G.C., Matson, P.A., Vitousek, P.M., 1997. Ecosystem services supplied by soil. *Nature’s services:*  
675 *societal dependence on natural ecosystems* 113–132.

676 David, F., 2010a. An example of the consequences of human activities on the evolution of subalpine  
677 landscapes. *Comptes Rendus Palevol* 9, 229–235. <https://doi.org/10.1016/j.crpv.2010.06.002>

678 David, F., 2010b. Expansion of green alder (*Alnus alnobetula* [Ehrh] K. Koch) in the northern French  
679 Alps: A palaeoecological point of view. *Comptes Rendus Biologies* 333, 424–428.  
680 <https://doi.org/10.1016/j.crv.2010.01.002>

681 Doyen, E., Etienne, D., 2017. Ecological and human land-use indicator value of fungal spore  
682 morphotypes and assemblages. *Vegetation History and Archaeobotany* 26, 357–367.  
683 <https://doi.org/10.1007/s00334-016-0599-2>

684 Egli, M., Dahms, D., Norton, K., 2014. Soil formation rates on silicate parent material in alpine  
685 environments: Different approaches—different results? *Geoderma* 213, 320–333.  
686 <https://doi.org/10.1016/j.geoderma.2013.08.016>

687 Enters, D., Dorfler, W., Zolitschka, B., 2008. Historical soil erosion and land-use change during the last  
688 two millennia recorded in lake sediments of Frickenhauser See, northern Bavaria, central  
689 Germany. *The Holocene* 18, 243–254. <https://doi.org/10.1177/0959683607086762>

690 Ewing, H.A., Nater, E.A., 2002. Holocene Soil Development on Till and Outwash Inferred from Lake-  
691 Sediment Geochemistry in Michigan and Wisconsin. *Quaternary Research* 57, 234–243.  
692 <https://doi.org/10.1006/qres.2001.2303>

693 FAO (Ed.), 2006. Guidelines for soil description, 4., [rev.] ed. ed. FAO, Rome.

694 Fouinat, L., Sabatier, P., Poulénard, J., Etienne, D., Crouzet, C., Develle, A.-L., Doyen, E., Malet, E.,  
695 Reyss, J.-L., Sagot, C., Bonet, R., Arnaud, F., 2017a. One thousand seven hundred years of  
696 interaction between glacial activity and flood frequency in proglacial Lake Muzelle (western  
697 French Alps). *Quaternary Research* 87, 407–422. <https://doi.org/10.1017/qua.2017.18>

698 Fouinat, L., Sabatier, P., Poulénard, J., Reyss, J.-L., Montet, X., Arnaud, F., 2017b. A new CT scan  
699 methodology to characterize a small aggregation gravel clast contained in a soft sediment  
700 matrix. *Earth Surface Dynamics* 5, 199–209. <https://doi.org/10.5194/esurf-5-199-2017>

701 Giguet-Covex, C., Arnaud, F., Enters, D., Poulénard, J., Millet, L., Francus, P., David, F., Rey, P.-J.,  
702 Wilhelm, B., Delannoy, J.-J., 2012. Frequency and intensity of high-altitude floods over the  
703 last 3.5ka in northwestern French Alps (Lake Anterne). *Quaternary Research* 77, 12–22.  
704 <https://doi.org/10.1016/j.yqres.2011.11.003>

705 Giguet-Covex, C., Arnaud, F., Poulénard, J., Disnar, J.-R., Delhon, C., Francus, P., David, F., Enters, D.,  
706 Rey, P.-J., Delannoy, J.-J., 2011. Changes in erosion patterns during the Holocene in a  
707 currently treeless subalpine catchment inferred from lake sediment geochemistry (Lake  
708 Anterne, 2063 m a.s.l., NW French Alps): The role of climate and human activities. *The  
709 Holocene* 21, 651–665. <https://doi.org/10.1177/0959683610391320>

710 Giguet-covex, C., Ficetola, F.G., Walsh, K.J., Poulénard, J., Bajard, M., Fouinat, L., Pierre, S., Gielly, L.,  
711 Messenger, E., Develle, A.-L., David, F., Taberlet, P., Brisset, E., Guiter, F., Sinet, R., Fabien, A.,  
712 2019. New insights on lake sediment DNA from the catchment: importance of taphonomic  
713 and analytical issues on the record quality (preprint). *EarthArXiv*.  
714 <https://doi.org/10.31223/osf.io/cnh3r>

715 Giguet-Covex, C., Pansu, J., Arnaud, F., Rey, P.-J., Griggo, C., Gielly, L., Domaizon, I., Coissac, E., David,  
716 F., Choler, P., Poulénard, J., Taberlet, P., 2014. Long livestock farming history and human  
717 landscape shaping revealed by lake sediment DNA. *Nature Communications* 5.  
718 <https://doi.org/10.1038/ncomms4211>

719 Giorgi, F., Torma, C., Coppola, E., Ban, N., Schär, C., Somot, S., 2016. Enhanced summer convective  
720 rainfall at Alpine high elevations in response to climate warming. *Nature Geoscience* 9, 584–  
721 589. <https://doi.org/10.1038/ngeo2761>

722 Goldberg, E.D., 1963. Geochronology with 210Pb. *Radioactive dating* 121–131.

723 Guffond, C., 2017. Sixt-Fer-à-Cheval (Haute-Savoie). *Alpage de Sales. Archéologie médiévale* 180.

724 Guffond, C., Mélo, A., 2018. Une institution collective dans l'histoire : l'alpage de Sales (Sixt-Fer-à-  
725 Cheval, Haute-Savoie, fin XIVE-fin XIXe siècles). *Etat et institutions en Savoie - Actes du 46e  
726 Cong. des Soc. Sav. de Savoie - 2016, Soc. d'Hist. et d'Archéologie de Maurienne, 2018* 253–  
727 266.

728 Heiri, O., Lotter, A.F., Lemcke, G., 2001. Loss on ignition as a method for estimating organic and  
729 carbonate content in sediments: reproducibility and comparability of results. *Journal of  
730 paleolimnology* 25, 101–110.

731 Holzhauser, H., Magny, M.J., Zumbühl, H.J., 2005. Glacier and lake-level variations in west-central  
732 Europe over the last 3500 years. *The Holocene* 15, 789–801.  
733 <https://doi.org/10.1191/0959683605hl853ra>

734 IPCC, 2019. IPCC Special Report on Climate Change and Land. An IPCC Special Report on climate  
735 change, desertification, land degradation, sustainable land management, food security, and  
736 greenhouse gas fluxes in terrestrial ecosystems.

737 Kaplan, J.O., Krumhardt, K.M., Ellis, E.C., Ruddiman, W.F., Lemmen, C., Goldewijk, K.K., 2011.  
738 Holocene carbon emissions as a result of anthropogenic land cover change. *The Holocene* 21,  
739 775–791. <https://doi.org/10.1177/0959683610386983>

740 Krishnaswamy, S., Lal, D., Martin, J.M., Meybeck, M., 1971. Geochronology of lake sediments. *Earth  
741 and Planetary Science Letters* 11, 407–414. [https://doi.org/10.1016/0012-821X\(71\)90202-0](https://doi.org/10.1016/0012-821X(71)90202-0)

742 Lal, R., 2003. Soil erosion and the global carbon budget. *Environment International* 29, 437–450.  
743 [https://doi.org/10.1016/S0160-4120\(02\)00192-7](https://doi.org/10.1016/S0160-4120(02)00192-7)

744 Le Roy, M., Nicolussi, K., Deline, P., Astrade, L., Edouard, J.-L., Miramont, C., Arnaud, F., 2015.  
745 Calendar-dated glacier variations in the western European Alps during the Neoglacial: the  
746 Mer de Glace record, Mont Blanc massif. *Quaternary Science Reviews* 108, 1–22.  
747 <https://doi.org/10.1016/j.quascirev.2014.10.033>

748 Magny, M., Bossuet, G., Ruffaldi, P., Leroux, A., Mouthon, J., 2011. Orbital imprint on Holocene  
749 palaeohydrological variations in west-central Europe as reflected by lake-level changes at  
750 Cerin (Jura Mountains, eastern France). *Journal of Quaternary Science* 26, 171–177.  
751 <https://doi.org/10.1002/jqs.1436>

752 Martini, J., 1966. Etude pétrographique des grés de Taveyanne entre Arve et Giffre ( Haute Savoie,  
753 France) . *Alpes (Theses)*. Université de Genève.

754 MEA, M.E.A., 2005. Ecosystems and human well-being: wetlands and water. World resources  
755 institute, Washington, DC 5.

756 Moreno, A., Valero-Garcés, B.L., González-Sampériz, P., Rico, M., 2008. Flood response to rainfall  
757 variability during the last 2000 years inferred from the Taravilla Lake record (Central Iberian  
758 Range, Spain). *Journal of Paleolimnology* 40, 943–961. <https://doi.org/10.1007/s10933-008-9209-3>

759

760 Mougín, P., 1914. Les torrents de la Savoie. La Fontaine de Siloé.

761 Mourier, B., Poulenard, J., Chauvel, C., Faivre, P., Carcaillet, C., 2008. Distinguishing subalpine soil  
762 types using extractible Al and Fe fractions and REE geochemistry. *Geoderma* 145, 107–120.  
763 <https://doi.org/10.1016/j.geoderma.2008.03.001>

764 Nicolussi, K., Kaufmann, M., Patzelt, G., Plicht van der, J., Thurner, A., 2005. Holocene tree-line  
765 variability in the Kauner Valley, Central Eastern Alps, indicated by dendrochronological  
766 analysis of living trees and subfossil logs. *Vegetation History and Archaeobotany* 14, 221–  
767 234. <https://doi.org/10.1007/s00334-005-0013-y>

768 Noren, A.J., Bierman, P.R., Steig, E.J., Lini, A., Southon, J., 2002. Millennial-scale storminess variability  
769 in the northeastern United States during the Holocene epoch. *Nature* 419, 821.

770 Parducci, L., Bennett, K.D., Ficetola, G.F., Alsos, I.G., Suyama, Y., Wood, J.R., Pedersen, M.W., 2017.  
771 Ancient plant DNA in lake sediments. *New Phytologist* 214, 924–942.  
772 <https://doi.org/10.1111/nph.14470>

773 R Development Core Team, 2011. R: A Language and Environment for Statistical Computing. R  
774 Foundation for Statistical Computing, Vienna, Austria.

775 Rapuc, W., Sabatier, P., Arnaud, F., Palumbo, A., Develle, A.-L., Reyss, J.-L., Augustin, L., Régnier, E.,  
776 Piccin, A., Chapron, E., Dumoulin, J.-P., von Grafenstein, U., 2019. Holocene-long record of  
777 flood frequency in the Southern Alps (Lake Iseo, Italy) under human and climate forcing.  
778 *Global and Planetary Change* 175, 160–172. <https://doi.org/10.1016/j.gloplacha.2019.02.010>

779 Reimer, P.J., Bard, E., Bayliss, A., Beck, J.W., Blackwell, P.G., Bronk Ramsey, C., Buck, C.E., Cheng, H.,  
780 Edwards, R.L., Friedrich, M., 2013. IntCal13 and Marine13 radiocarbon age calibration curves  
781 0-50,000 years cal BP.

782 Rey, P.-J., 2010. Passy-Servoz. Les premières occupations humaines des versants du col d’Anterne.  
783 *Bilan scientifique de la Région Rhône-Alpes* 198–200.

784 Rey, P.-J., 2008. Premières occupations de la montagne sur les versants du col d’Anterne (2 257 m).  
785 *ADLFI. Archéologie de la France- Informations. une revue Gallia*.

786 Rey, P.-J., Batigne-Vallet, C., Collombet, J., Delhon, C., Martin, L., Moulin, B., Poulenard, J.,  
787 Scoccimaro, N., Sordoillet, D., Thiebault, S., others, 2008. Approche archéologique et  
788 environnementale des premiers peuplements alpins autour du col du Petit Saint-Bernard  
789 (Savoie, Vallée d’Aoste): un bilan d’étape, in: *Archéologie de l’espace Montagnard:*  
790 *Confrontation d’expériences Européennes*. pp. 197–210.

791 Reyss, J.-L., Schmidt, S., Legeleux, F., Bonté, P., 1995. Large, low background well-type detectors for  
792 measurements of environmental radioactivity. *Nuclear Instruments and Methods in Physics*

793 Research Section A: Accelerators, Spectrometers, Detectors and Associated Equipment 357,  
794 391–397.

795 Robbins, J.A., Edgington, D.N., 1975. Determination of recent sedimentation rates in Lake Michigan  
796 using Pb-210 and Cs-137. *Geochimica et Cosmochimica Acta* 39, 285–304.

797 Sabatier, P., Bruno, W., Francesco, F.G., Fanny, M., Jérôme, P., Anne-Lise, D., Adeline, B., Wentao, C.,  
798 Cécile, P., Jean-Louis, R., Ludovic, G., Manon, B., Yves, P., Emmanuel, M., Pierre, T., Fabien,  
799 A., 2017. 6-kyr record of flood frequency and intensity in the western Mediterranean Alps –  
800 Interplay of solar and temperature forcing. *Quaternary Science Reviews* 170, 121–135.  
801 <https://doi.org/10.1016/j.quascirev.2017.06.019>

802 Sesiano, J., 1993. Monographie physique des plans d'eau naturels du département de la Haute-  
803 Savoie, France.

804 Shand, C.A., Wendler, R., 2014. Portable X-ray fluorescence analysis of mineral and organic soils and  
805 the influence of organic matter. *Journal of Geochemical Exploration* 143, 31–42.  
806 <https://doi.org/10.1016/j.gexplo.2014.03.005>

807 Stacy, E.M., Hart, S.C., Hunsaker, C.T., Johnson, D.W., Berhe, A.A., 2015. Soil carbon and nitrogen  
808 erosion in forested catchments: implications for erosion-induced terrestrial carbon  
809 sequestration. *Biogeosciences* 12, 4861–4874. <https://doi.org/10.5194/bg-12-4861-2015>

810 Sturm, M., Matter, A., 1978. Turbidites and varves in Lake Brienz (Switzerland): deposition of clastic  
811 detritus by density currents. Wiley Online Library.

812 Talon, B., 2006. Analyses anthracologiques au col du Petit St-Bernard. *Archéoanthracologie et*  
813 *pédoanthracologie.*, in: *Actes Du Séminaire de Clôture Du Programme INTERREG III A*  
814 *ALCOTRA 2000-2006: Alpis Graia. Archéologie sans Frontière Au Col Du Petit St-Bernard.*  
815 *Aoste*, pp. 51–58.

816 Vanmaercke, M., Poesen, J., Govers, G., Verstraeten, G., 2015. Quantifying human impacts on  
817 catchment sediment yield: A continental approach. *Global and Planetary Change* 130, 22–36.  
818 <https://doi.org/10.1016/j.gloplacha.2015.04.001>

819 Verheijen, F.G.A., Jones, R.J.A., Rickson, R.J., Smith, C.J., 2009. Tolerable versus actual soil erosion  
820 rates in Europe. *Earth-Science Reviews* 94, 23–38.  
821 <https://doi.org/10.1016/j.earscirev.2009.02.003>

822 Wang, Z., Hoffmann, T., Six, J., Kaplan, J.O., Govers, G., Doetterl, S., Van Oost, K., 2017. Human-  
823 induced erosion has offset one-third of carbon emissions from land cover change. *Nature*  
824 *Climate Change* 7, 345–349. <https://doi.org/10.1038/nclimate3263>

825 Wick, L., van Leeuwen, J.F., van der Knaap, W.O., Lotter, A.F., 2003. Holocene vegetation  
826 development in the catchment of Sägistalsee (1935 m asl), a small lake in the Swiss Alps.  
827 *Journal of Paleolimnology* 30, 261–272.

828 Wilhelm, B., Arnaud, F., Sabatier, P., Crouzet, C., Brisset, E., Chaumillon, E., Disnar, J.-R., Guiter, F.,  
829 Malet, E., Reyss, J.-L., Tachikawa, K., Bard, E., Delannoy, J.-J., 2012. 1400years of extreme  
830 precipitation patterns over the Mediterranean French Alps and possible forcing mechanisms.  
831 *Quaternary Research* 78, 1–12. <https://doi.org/10.1016/j.yqres.2012.03.003>

832 Wilhelm, B., Ballesteros Canovas, J.A., Corella Aznar, J.P., Kämpf, L., Swierczynski, T., Stoffel, M.,  
833 Støren, E., Toonen, W., 2018. Recent advances in paleoflood hydrology: From new archives  
834 to data compilation and analysis. *Water Security* 3, 1–8.  
835 <https://doi.org/10.1016/j.wasec.2018.07.001>

836 Wilhelm, B., Ballesteros Cánovas, J.A., Macdonald, N., Toonen, W.H.J., Baker, V., Barriendos, M.,  
837 Benito, G., Brauer, A., Corella, J.P., Denniston, R., Glaser, R., Ionita, M., Kahle, M., Liu, T.,  
838 Luetscher, M., Macklin, M., Mudelsee, M., Munoz, S., Schulte, L., St. George, S., Stoffel, M.,  
839 Wetter, O., 2019. Interpreting historical, botanical, and geological evidence to aid  
840 preparations for future floods. *WIREs Water* 6, e1318. <https://doi.org/10.1002/wat2.1318>

841 Wirth, S.B., Glur, L., Gilli, A., Anselmetti, F.S., 2013. Holocene flood frequency across the Central Alps  
842 – solar forcing and evidence for variations in North Atlantic atmospheric circulation.  
843 *Quaternary Science Reviews* 80, 112–128. <https://doi.org/10.1016/j.quascirev.2013.09.002>

844 WRB - FAO, 2014. World reference base for soil resources 2014 international soil classification  
845 system for naming soils and creating legends for soil maps. FAO, Rome.  
846

847